AFRL-SR-BL-TR-01-

0109

REPORT DOCUMENTATION PAGE

Public reporting burden for this collection of information is estimated to average 1 hour per response, including the time for reviewing instructions, searching existing data sources, gathering and maintaining the data needed, and completing and reviewing this collection of information. Send comments regarding this burden estimate or any other aspect of this collection of information, including suggestions for reducing this burden to Washington Headquarters Services, Directorate for Information Operations and Reports, 1215 Jefferson Davis Highway, Suite 1204, Arlington, VA 22202-4302, and to the Office of Management and Budget, Paperwork Reduction Project (0704-0188), Washington, DC 20503

1. AGENCY USE ONLY (Leave blank)	2. REPORT DATE	3. REPORT TYPE AND DATES COVERED
	01/31/01	Final technical report, 11/01/97-10/31/00

4. TITLE AND SUBTITLE
Energy Transfer Kinetics and Dynamics of Relevance to Iodine Lasers

5. FUNDING NUMBERS
61102F 2303 ES

6. AUTHOR(S)
Michael C. Heaven

7. PERFORMING ORGANIZATION NAME(S) AND ADDRESS(ES)

Emory University
1784 N. Decatur Road
Suite 510
Atlanta, GA 30322

8. PERFORMING ORGANIZATION REPORT NUMBER

9. SPONSORING / MONITORING AGENCY NAME(S) AND ADDRESS(ES)

AFOSR/NL
801 N. Randolph Street
Suite 732
Arlington, VA 22203-1977

10. SPONSORING / MONITORING AGENCY REPORT NUMBER
F49620-98-1-0054

11. SUPPLEMENTARY NOTES

AIR FORCE OFFICE OF SCIENTIFIC RESEARCH (AFOSR)
NOTICE OF TRANSMITTAL DTIC. THIS TECHNICAL REPORT
HAS BEEN REVIEWED AND IS APPROVED FOR PUBLIC RELEASE
LAW AFR 190-12. DISTRIBUTION IS UNLIMITED.

12a. DISTRIBUTION / AVAILABILITY STATEMENT
APPROVED FOR PUBLIC RELEASE: DISTRIBUTION IS UNLIMITED

12b. DISTRIBUTION CODE

13. ABSTRACT ***(Maximum 200 Words)***

Rate constants were measured for elementary reactions that are of importance for iodine chemical lasers driven by $O_2(a^1\Delta)$ (COIL) or $NCl(a^1\Delta)$. Energy transfer between $I(^2P_{1/2})$ and $O_2(X)$ has been studied in detail. Rate constants for electronic energy transfer and nuclear spin relaxation were measured over the temperature range from 150-300K. The mechanism for dissociation of I_2 in COIL systems has been examined using kinetic models and experimental studies of $I_2(A')$ collisional deactivation. A new model for the dissociation mechanism is presented.

Quenching of $NCl(a)$ has been characterized for the collision partners O_2, Cl_2, HCl, H_2, I_2, and ClN_3. These measurements resolved serious discrepancies that had emerged from earlier investigations. Removal of $NCl(a)$ by I_2 was found to be a reactive process that liberates I atoms. The second order rate constant for self-annihilation of $NCl(a)$ was measured using time-resolved fluorescence techniques. The value obtained, $(7\pm2)\times10^{-13}$ cm^3 s^{-1} is an order of magnitude slower than pervious estimates.

Detection of $NCl(X)$ by means of the b-X absorption bands was demonstrated. Time-resolved absorption measurements were used to examine the kinetics of $NCl(X)$ formation and decay.

14. SUBJECT TERMS
Energy transfer, Chemical lasers, COIL, NCl metastables.

15. NUMBER OF PAGES
43

16. PRICE CODE

17. SECURITY CLASSIFICATION OF REPORT	18. SECURITY CLASSIFICATION OF THIS PAGE	19. SECURITY CLASSIFICATION OF ABSTRACT	20. LIMITATION OF ABSTRACT
UNCLASSIFIED	UNCLASSIFIED	UNCLASSIFIED	

NSN 7540-01-280-5500

Standard Form 298 (Rev. 2-89)
Prescribed by ANSI Std. Z39-18
298-102

20010305 067

Contents

1. Overview

Studies of elementary reactions that are of importance in chemical iodine lasers were the primary focus of the work described in this report. One motivation for these studies was provided by the need to achieve a better understanding of the kinetics of Chemical Oxygen Iodine Laser (COIL). The pump reaction of this device,

$$O_2(a^1\Delta) + I(^2P_{3/2}) \leftrightarrow O_2(X^3\Sigma^-) + I(^2P_{1/2}) \quad (1)$$

was studied at low temperature (T=150 K) to provide rate constant data suitable for modeling supersonic lasers[1,2]. This reaction was also investigated using high level theoretical methods, in order to test the ability of such models to predict electronic energy transfer kinetics[3,4].

Iodine lasers operate on a single hyperfine of the $^2P_{1/2}$-$^2P_{3/2}$ transition (F'=3→F"=4). As a consequence, power extraction is influenced by the rate at which collisions transfer population between the F'=2 and F'=3 sub-levels of $^2P_{1/2}$. The hyperfine transfer rate constants had not been measured previously, and most models of COIL systems have assumed that the process is fast enough to maintain equilibrium populations in the F'=2 and 3 sub-levels. In the present work we performed the first direct measurements of the hyperfine transfer rate constants over the temperature range from 10 – 300 K[1,2]. The rate constants were smaller than had been assumed, indicating that computational simulations of COIL should include specific treatment of hyperfine relaxation.

Characterizations of a prototype supersonic COIL device (VertiCOIL) revealed cavity temperatures that were appreciably greater than the value predicted by computational fluid dynamics models[5]. It was suggested that the heat release was due to either condensation of H_2O in expansion or quenching of $I(^2P_{1/2})$ by H_2O. Experiments designed to test both of these possibilities were carried out. The results did not support either hypothesis.

The mechanism by which I_2 is dissociated by $O_2(a^1\Delta)$ is one of the least well understood aspects of COIL systems[6]. It has been estimated that somewhere between four and six $O_2(a)$ molecules are needed to dissociate one I_2 molecule, but the details of the process remain obscure. We have investigated kinetic models of the dissociation process that identify vibrationally excited $I_2(X)$ as the key intermediate species[7]. We were unable construct satisfactory models based on this mechanism, and have proposed a modified scheme that involves electronically excited I_2 (a variant of models originally proposed by Bacis and co-workers[8]). Measurements of quenching rate constants for the *A'* state of I_2 were carried out to obtain parameters for this model. The revised mechanism provides a better quantitative description of the dissociation kinetics.

Iodine lasers that are driven by energy transfer from NCl(a) are currently being developed[9-11]. Measurements of the rate constants for quenching and reaction of NCl(a) are needed to guide the design and development of such devices. Earlier studies of NCl(a) quenching yielded rate constants that were strongly dependent on the technique used to perform the measurement[12-14]. In some instances different techniques yielded rate constants that differed by more than an order of magnitude. New measurements were performed to resolve these conflicts and provide data for previously unexamined collision partners[15]. Self-annihilation of NCl(a) was one of the most significant processes examined. This second order reaction limits the concentration of NCl(a) that can be generated by chemical means and dominates the transport losses. We obtained a self-annihilation rate constant of $(7\pm2)\times10^{-13}$ cm^3 s^{-1}, which is a factor of ten smaller than the previous estimate[13]. This result is encouraging for NCl(a) transfer lasers as it indicates that transport and mixing losses will be less sever than earlier kinetic models had predicted.

Quenching of NCl(a) by I_2 was found to be a reactive process that liberates atomic I. Subsequently, the electronic energy transfer process $I(^2P_{3/2})+NCl(a) \rightarrow I(^2P_{1/2})+NCl(X)$ lead to emission from atomic iodine. Analysis of the temporal behavior of the iodine fluorescence indicated that quenching of $I(^2P_{1/2})$ by ClN_3 (the NCl(a) precursor) was very slow. This was confirmed in a study of the quenching of $I(^2P_{1/2})$ by ClN_3 and HN_3.

A method for observing NCl(X) by means of the b-X absorption bands was developed[15]. This is of interest as absorption measurements may be used to characterize the temperature and pressure conditions within the cavity of an NCl(a)/I laser system. The absorption measurements were carried out in collaboration with Dr. G. C. Manke II (AFRL, NM) and Dr. S. J. Davis (PSI, MA). The results are being used in the design of a diagnostic instrument for the AFRL azide laser flow facility. Time-resolved NCl(X) absorption measurements were used to determine the yield of NCl(a) from ClN_3 photolysis.

Theoretical studies of I+NCl(a) energy transfer and the reaction $Cl+N_3 \rightarrow NCl(a,X)+N_2$ were initiated in a collaborative effort with Professor K. Morokuma. The main objective of these projects is to determine product branching ratios. The efficiency of an NCl(a)/I laser system is dependent on these branching ratios, which are difficult to measure accurately by experimental means. For I+NCl(a) the potential energy surfaces have been calculated, and the surface intersections responsible for electronic energy transfer have been located. As the relevant potentials do not correspond to chemically bound states, it appears that energy transfer occurs by a purely physical mechanism. Calculations for the $Cl+N_3$ reaction have been used to locate the barriers to formation of singlet (NCl(a)+N_2) and triplet (NCl(X)+N_2) products. Both barriers lie below the energy of the entrance channel. From the energetics alone we cannot explain the observed preference for

formation of the singlet product. Dynamical calculations are planned that will probe this question in more detail.

2. Studies of $I(^2P_{1/2})+O_2$ Energy Transfer.

2a. Experimental studies of electronic energy transfer and nuclear spin state changing collisions.

The energy transfer process

$$O_2(a^1\Delta) + I(^2P_{3/2}) \leftrightarrow O_2(X^3\Sigma^-) + I(^2P_{1/2}) \quad (1)$$

is exothermic by 0.8 kcal mol^{-1} (E/R=401.4 K) in the forward direction. For the purpose of modeling COIL kinetics, rate constants for both the forward and backward transfer steps are needed. In practice, the rate constant for the reverse reaction (k_b) is most easily measured. It is known that the quenching of I* (= $I(^2P_{1/2})$) by $O_2(X)$ is dominated by the E-E energy transfer process. Hence, measurements of the quenching rate constant yield good estimates for k_b. Once k_b is known, the forward rate constant (k_f) can be calculated reliably from the theoretical expression for the equilibrium constant. Rate constants for the forward and backward transfer at room temperature are well established. However, for the purpose of modeling supersonic COIL devices, knowledge of the temperature dependence of the rate constants over the range $150 \leq T \leq 300$ K is needed.

In this program we characterized I* + O_2 energy transfer at temperatures near 150 K. As in our previous work on this system[16], a Laval nozzle expansion was used to generate low temperature gas flows. I* was produced by pulsed photolysis of I_2. Two different time-resolved techniques were used to determine the rate constant for energy transfer from I* to O_2. Initially a fast IR detector was used to observe I* fluorescence decay curves. Measurements of the decay rate as a function of O_2 concentration yielded a transfer rate constant of $k_b(150)=(6.3\pm1.0)\times10^{-12}$ cm^3 s^{-1}. This value was somewhat higher than our previous determination[16] of $k_b(150)=(4.6\pm1.0)\times10^{-12}$ cm^3 s^{-1} (measurements that involved deconvolution of signals from a slow Ge detector).

Pulsed LIF detection of I* was used for the second series of measurements. Our initial attempts with this method yielded an energy transfer rate constant of $k_b(150)=(7.6\pm1.0)\times10^{-12}$ cm^3 s^{-1}. We speculated that the discrepancy between the rate constants derived from LIF and IR fluorescence may be indicative of systematic errors in the former. Further investigation of this discrepancy revealed a rather surprising aspect of $I_2(B)$ photolysis.

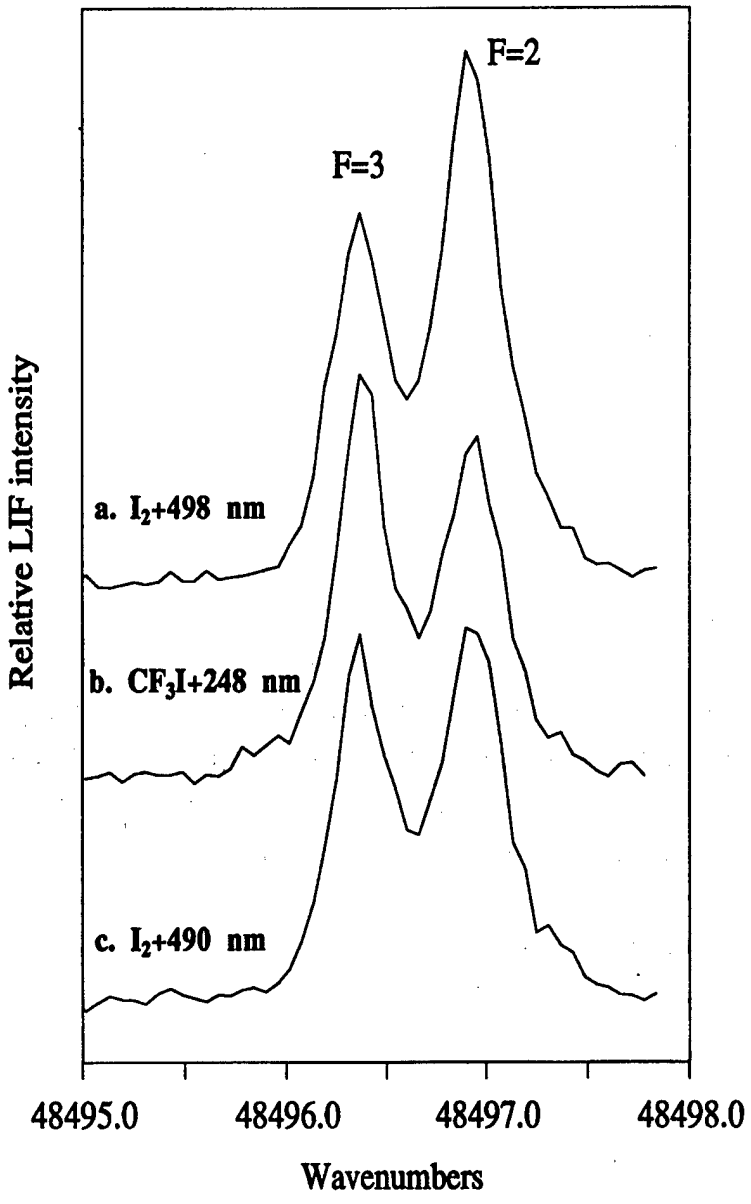
F=2
F=3
a. I_2+498 nm
b. CF_3I+248 nm
c. I_2+490 nm
Relative LIF intensity
48495.0
48496.0
48497.0
48498.0
Wavenumbers

Figure 1

In the LIF experiments, I* was detected by exciting the $5p^46s$ ($^2P_{3/2}$) - $5p^5$ ($^2P_{1/2}$) transition. Owing to the large hyperfine splitting of the $^2P_{1/2}$ state, the spectrum shows two resolved features, corresponding to transitions from the I* F=2 and F=3 sub-levels. Fig. 1 shows spectra taken using three different methods for production of I*. The upper and lower traces correspond to photolysis of I_2 at 498 nm and 490 nm, respectively. The center trace was obtained when I* was generated by 248 nm photolysis of CF_3I. It is apparent from these traces that the different photolysis sources yielded different initial populations in the atomic hyperfine sub levels. Photolysis of CF_3I is known to result in statistical population of the I* hyperfine levels (i.e., [F=3]/[F=2] = 7/5). This distribution is evident in the center trace of Fig. 1. The upper trace shows that 498 nm photolysis of I_2 results in preferential population of F=2.

When quenching of I* by O_2 was investigated using 498 nm photolysis, the kinetics of the F=2 and F=3 sub levels appeared to be different. For example, Fig. 2 shows the effect of adding O_2 to the expansion. This trace gives the impression that F=2 is quenched, while F=3 is not affected. It is most unlikely that the hyperfine sub-levels are quenched with different rate constants. The most probable explanation for this behavior is that the quenching rate constants for the hyperfine sub-levels are the same, but the kinetics are complicated by transfer between the hyperfine levels (initially, transfer from F=2 to F=3). Kinetic modeling of the data supported this interpretation. Analysis of the LIF data yielded an electronic energy transfer rate constant of $k_b(150)=7.3\times10^{-12}$, and hyperfine transfer rate constants of $k(2\rightarrow3)=2.5\times10^{-11}$ and $k(3\rightarrow2)=1.8\times10^{-11}$ cm^3 s^{-1}. In accordance with theoretical predictions, we found that the closed-shell collision partners He, Ar, and N_2 did not induce measurable degrees of hyperfine relaxation under the conditions of our experiments.

For I*+$O_2(X)$ an optimized fit to both the IR fluorescence and LIF data gave rate constants of $k_b(150)=(7.0\pm0.7)\times10^{-12}$, $k(2\rightarrow3)=2.6\times10^{-11}$ and $k(3\rightarrow2)=1.9\times10^{-11}$ cm^3 s^{-1}. The revised value for $k_b(150)$ was significantly below the rate constants predicted by currently accepted models. When combined with the room temperature value for k_b, the present result is consistent with the Arrhenius expression

$$k_b(T) = 1.05\times10^{-10}\exp(-401.4/T)\ cm^3\ s^{-1}$$

The rate constant for $O_2(a)$+I $\rightarrow$ $O_2(X)$ + I* was derived from this expression via the statistical mechanics expression for the equilibrium constant. A temperature independent value of $k_f=7.8\times10^{-11}$ cm^3 s^{-1} was obtained. Further studies were carried out to characterize the temperature dependence of the I*(F)+$O_2(X)$ $\rightarrow$I*(F')+$O_2(X)$ hyperfine transfer process. To augment energy transfer data taken at 150 K, measurements were made at

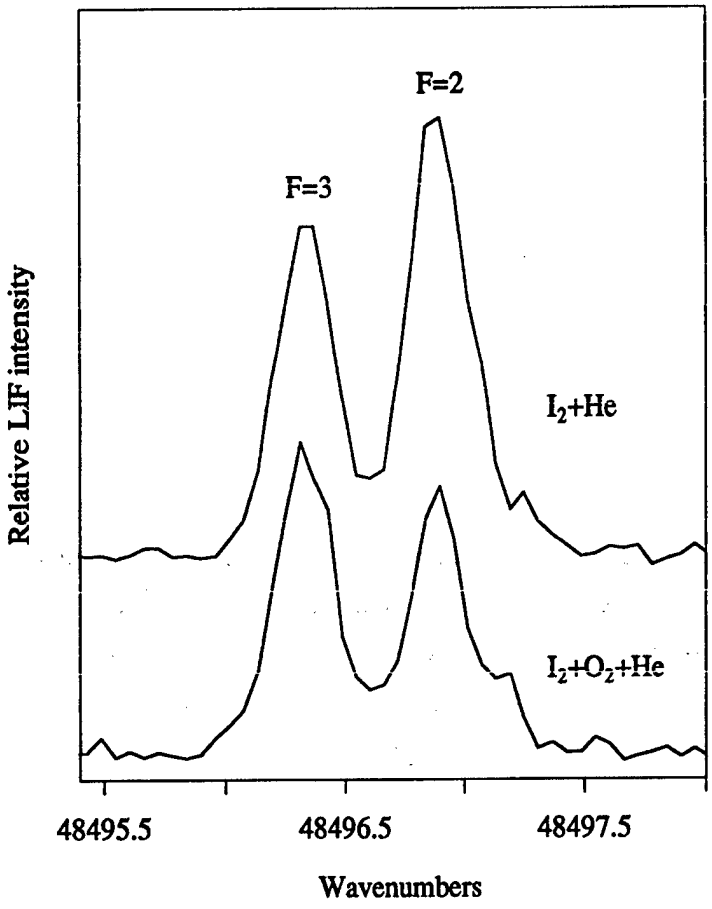
F=2
F=3
I_2+He
I_2+O_2+He
Relative LIF intensity
48495.5
48496.5
48497.5
Wavenumbers

Figure 2

10 K, in a free-jet expansion, and 295 K in a conventional vacuum system. As part of this investigation we characterized the nascent I* hyperfine level population distributions resulting from photolysis of I_2 at different temperatures and wavelengths.

Nascent I* population distributions resulting from photolysis of jet-cooled I_2 (10 K) were examined for several photolysis wavelengths in the 490-499 nm range. Examples of the I* LIF spectra are shown in Fig. 3. As the photolysis wavelength increased from 490 to 499 nm, the probability for populating the F=3 level decreased dramatically. Note that 499 nm corresponds to the onset of the *B-X* continuum. The lower trace in Fig. 3 shows that dissociation at energies just above the *B* state dissociation threshold strongly favored formation of F=2 products. Population transfer between hyperfine levels is most easily observed when the initial population distribution is far from equilibrium. Consequently, 499 nm photolysis was used for energy transfer measurements. Fig. 4 shows spectra taken in the free-jet, with and without O_2 present. Comparing these traces, it can be seen that collisions with O_2 are, on average, moving population from F=2 to F=3. At the local temperature of these measurements, the rate constant for electronic quenching of I* by O_2 should be negligibly slow (the main channel, transfer to $O_2(a)$, is exothermic by 278 cm^{-1}). Analysis of these data yielded rate constants of $k(2\rightarrow3)=2.0\pm0.5\times10^{-11}$ and $k(3\rightarrow2)=1.4\pm0.5\times10^{-11}$ $cm^3 s^{-1}$ at T=10 K.

Nascent I* distributions resulting from I_2 photolysis at room temperature were also non-statistical, but the effect was not as pronounced as it was for photolysis at 10 or 150 K. As for the low-temperature experiments, the relative population of F=3 decreased with increasing wavelength. At the long wavelength limit (499 nm) the [F=3]/[F=2] population ratio was approximately 2/3. Although electronic quenching was as fast as hyperfine transfer at room temperature, the latter was still readily observable. Kinetic modeling of the room temperature data defined rate constants of $k(2\rightarrow3)=(2.3\pm0.5)\times10^{-11}$ and $k(3\rightarrow2)=(1.6\pm0.5\times10^{-11})$ $cm^3 s^{-1}$. The hyperfine transfer rate constants were found to have no discernable temperature dependence over the range 10-295 K. As the hard-sphere collision frequency decreases with temperature, this suggests that the transfer cross sections increase with decreasing temperature.

For computational models of COIL systems it is usually assumed that hyperfine transfer is a rapid process. The relative populations in the F=2 and F=3 sub-levels are fixed at the equilibrium value, and it is assumed that the energy stored by I*(F=2) is available through hyperfine transfer. Our measurements show that the hyperfine transfer rate constants are smaller than theoretical estimates, and that the equilibrium assumption is not justified.

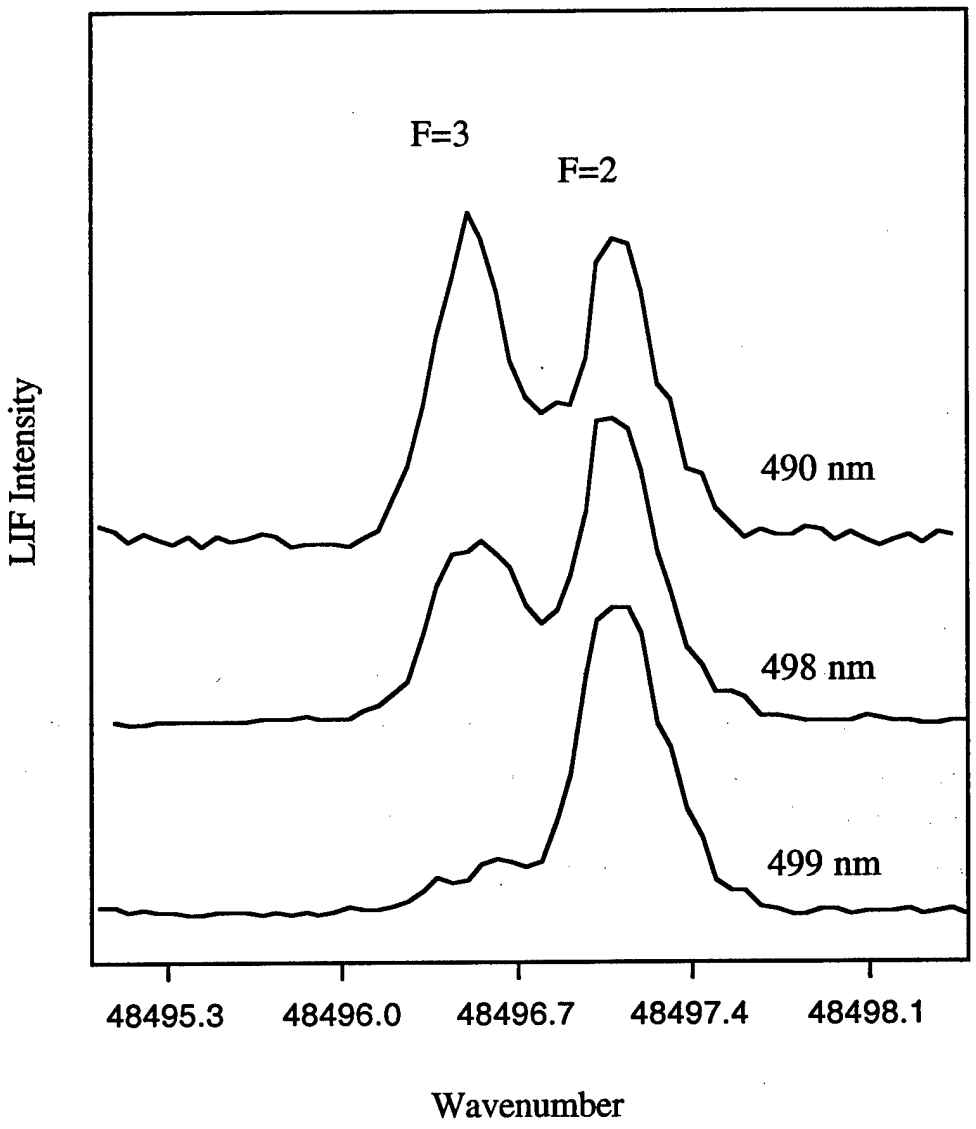

Figure 3. I* LIF spectra for photolysis of I_2 at 490, 498, and 499 nm. These data were taken at 10 K in an He expansion with a photolysis - probe delay of400 ns.

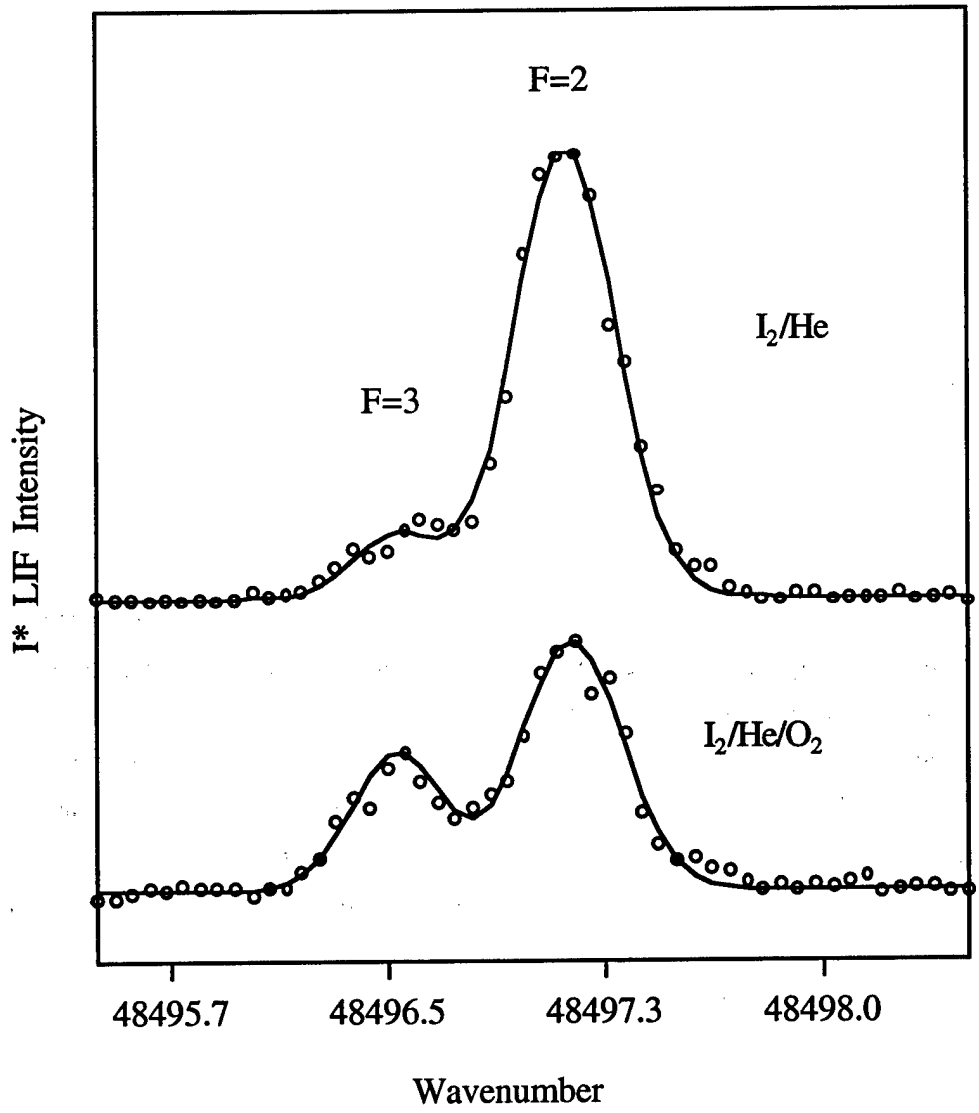

Figure 4. I* LIF spectra for photolysis of I_2 at 499 nm in a free-jet expansion. The upper trace shows the nascent population distribution of the hyperfine sub-levels. The lower trace shows the effect of adding O_2 to the expansion. Both traces were recorded using a photolysis-probe delay of 800 ns.

2b. Comment on the photodissociation dynamics of $I_2(B)$.

The non-statistical population of I* hyperfine levels produced by $I_2(B)$ photolysis was an unexpected result. In the absence of electronic state perturbations, dissociation of $I_2(B)$ should yield a statistical distribution. The observed distributions were consistent with electronic state mixings that are mediated by the $\hat{J}\cdot\hat{I}$ term in the molecular Hamiltonian. This operator can mix states that differ in Ω by ±1, and, in the process, break the *u/g* symmetry of the molecule. Such symmetry-breaking perturbations near the $I_2(B)$ dissociation limit have been observed previously[17]. Avoided crossings between curves that correlate with I*(F=2)+I and I*(F=3)+I can influence the final state population distribution, provided that the atoms move relatively slowly through crossing regions (adiabatic curve following). The fact that the lower energy hyperfine level receives the most population is consistent with an avoided crossing model. Note that the strong preference for population of F=2 seen for 499 nm photolysis of the 10 K sample (lower trace in Fig. 3) is not simply an energetic threshold effect. The photon energy is above the I*(F=3)+I dissociation limit.

As the velocity at which the I atoms traverse the curve crossings increases, the dynamics switch from adiabatic to diabatic curve following. Hence, as the photolysis wavelength is decreased, the hyperfine population distribution moves toward the statistical limit. This trend is evident in Fig. 3. For a fixed photolysis wavelength, the nascent distribution clearly exhibits a dependence on temperature. As the temperature increases, the $[2]_0/[3]_0$ ratio decreases. This behavior may also be explained by a curve crossing model. Thermal energy simply adds to the energy imparted by the photon, and thereby increases the final recoil velocity. Consequently, the $[2]_0/[3]_0$ ratio observed for 495 nm photolysis at 10 K was very similar to that seen for 498 nm photolysis at 150 K.

In future experiments it will be of interest to probe the nascent distribution of I $^2P_{3/2}$ hyperfine levels populated by I_2 *B* state photolysis. The distributions among these levels may also be non-statistical. If this proves to be the case, near-threshold photolysis of $I_2(B)$ may provide a convenient method for studying hyperfine relaxation of ground state atoms.

2c. Theoretical calculation of the rate constants for $I(^2P_{3/2}) + O_2(a^1\Delta_g) \Leftrightarrow I(^2P_{1/2}) + O_2(X^3\Sigma_g)$ (collaboration with Prof. K. Morokuma).

Theoretical studies of the I+$O_2(a)$ energy transfer process were performed to obtain a deeper understanding of the factors that determine the temperature dependence of the rate constant. This system also provides a challenging test of current theoretical methods.

Two dimensional potential energy surfaces for $I(^2P_{1/2}) + O_2(X)$ and $I(^2P_{3/2}) + O_2(a)$ were calculated using high-level *ab initio* methods (CASSCF followed by CASPT2 with the *cc-aug-pvtz* basis set)[4]. The O-O bond was held fixed at the centroid value. The Jacobi coordinates that describe the position of the I atom relative to the O-O bond (R and γ) were varied to generate a grid of energy points for each electronic state. Seven potential surfaces were obtained and then fitted exactly with simple analytical functions of the type

$$V_{ij}(\gamma, R) = \sum_{l=0,2,\ldots}^{18} c_l^{ij}(R)\overline{P}_l(\cos(\gamma)) \tag{2}$$

where $c_l^{ij}(R)$ are radially dependent expansion coefficients interpolated using 1-D splines, and $\overline{P}_l(\cos(\gamma))$ are normalized Legendre polynomials. The indices i and j denote the electronic state. Diabatic coupling elements connecting different pairs of states $i \neq j$ were calculated on the same grid, and fitted with the same type of analytical functions[3].

To a good approximation, we can treat the nuclear dynamics classically since we are dealing with interactions of heavy particles. Hamilton's equations of motion were solved to propagate the position of the nuclei in time according to the momenta, P (radial) and j (O_2 rotation).

$$H_{kk} = \frac{P^2}{2\overline{\mu}} + \frac{j^2}{2\mu r_c^2} + \frac{(J-j)^2}{2\overline{\mu}R^2} + V_{kk}(\gamma, R) \tag{3}$$

Eq. (3) is the Hamiltonian for the k-th potential, where $\overline{\mu}$ is the reduced mass of the collision complex, μ is reduced mass of O_2 and J is the total rotational angular momentum. The corresponding equations of motion for coordinates and conjugate momenta were integrated using a fourth order Runge-Kutta algorithm.

The electronic degrees of freedom must be treated quantum mechanically. For these calculations we used the surface hopping trajectory methods developed by Tully[18]. Electron densities were propagated via the time-dependent Schrödinger equation:

$$i\hbar\frac{da_{kj}}{dt} = \sum_l \left(a_{lj}V_{kl} - a_{kl}V_{lj}\right) \tag{4}$$

where the complex coefficients a_{kj} are amplitudes whose squared diagonal elements are populations, and off-diagonal elements are coherences. The nuclei and electron densities were propagated simultaneously, and transition probabilities were calculated according to Tully's[18] "fewest switches" model.

To calculate the temperature dependence of the rate constant for $I(^2P_{3/2}) + O_2(a^1\Delta_g) \rightarrow I(^2P_{1/2}) + O_2(X^3\Sigma_g^-)$ approximately 5×10^5 trajectories were statistically averaged over a range of impact parameters and collision energies. Temperatures in the range 10-300 K were investigated. It was found that collisions resulting in energy transfer were dominated by single hop trajectories. The calculated energy transfer rate constant decreased smoothly with increasing temperature over the range 100-300 K. The predicted value was in excellent agreement with the experimental result for 150 K, but the calculations underestimate room temperature data by a factor of 1.6. The rate constant increases with decreasing energy because (i) long-range attractive forces draw slow moving collision partners together and, (ii) the longer duration of slow collisions increases the probability of surface-hopping. It was also found that there is a competition between rotational relaxation of $O_2(a)$ and electronic energy transfer.

Given the complexity of this system we considered that the level of agreement between theory and experiment was very encouraging. The causes of the residual discrepancies could be related to errors in the potential energy surfaces and neglect of quantum interference effects.

4. Measurements related to heat release due to H_2O in COIL systems.

Studies of the VertiCOIL laser system at Kirtland AFB revealed unexpectedly high cavity temperatures[5]. Model calculations predicted downstream temperatures of 160 K, whereas the measured values were around 220 K. This was a matter of concern for the groups who simulate COIL systems, as the discrepancy could be indicative of serious problems in the fluid dynamics model. Dr. P. Crowell and co-workers at Logicon RDA (NM) speculated that condensation of H_2O in the supersonic expansion might be responsible for the downstream heating. Inclusion of this process in their model could reproduce the observed temperatures, but only when it was assumed that all of the H_2O in the flow condensed. The groups at both Kirtland AFB and Logicon RDA requested experimental investigation of this problem.

We searched for the condensation heating effect by observing the temperature in a $He/I_2/H_2O$ supersonic expansion as a function of added H_2O. The 2-D Laval nozzle apparatus described in reference 1 was used for these experiments. Two sample bombs, each filled with about 40ml of distilled water, and a sample cell containing solid I_2 were added to the inlet system. The sample holders were configured to pass the helium over the H_2O and then entrain I_2. For measurements of I_2/He alone, water vapor was removed from the flow by either bypassing the sample bombs or using a dry ice/acetone mixture to trap the water vapor. Both methods proved equally effective. The amount of water vapor added

was varied between 0 and 300 mTorr (downstream), as determined by monitoring the increase in the pressure of the expansion.

The temperature of the expansion with and without the addition of water vapor was estimated spectroscopically by using a dye laser to excite the *B-X* (14-0, 17-1) transitions of I_2. The relative intensities of the rotational and vibrational transitions were simulated to estimate the local temperature of the expansion. The temperature was determined 1 cm and 4 cm downstream from the throat of the nozzle. Typically the plenum pressure was around 10 Torr, resulting in a downstream pressure of about 2 Torr. Due to the limitations of our pumps, we were unable to use plenum pressures much above 10 Torr. Using the highest H_2O partial pressure we could achieve (300 mTorr downstream) and the maximum plenum pressure, we were unable to detect any heating effects due to the presence of H_2O.

As an alternative means of explaining the high temperature, it was proposed that quenching of I* by H_2O

$$I^* + H_2O \rightarrow I + H_2O \qquad \{48\}^a$$

might be responsible for the heat release. However, the rate constant for this process would have to be greater than the accepted value for this explanation to be viable. At the request of Dr. Gordon Hager (AFRL, Kirtland AFB) and Dr. Peter Crowell we re-examined the rate constant for reaction {48}. Measurements were made at room temperature under slow flow conditions. We obtained a quenching rate constant of $k_6 = (2.4 \pm 0.5) \times 10^{-12}$ $cm^3 sec^{-1}$, in excellent agreement with the results of several previous studies.

We attempted to explore the possibility that the rate constant for reaction {48} might increase with decreasing temperature. Unfortunately, it proved to be very difficult to obtain stable H_2O concentrations in the Laval expansion, and we were unable to make a reliable rate constant determination at 150 K. However, the results were not consistent with a dramatic increase in the rate constant in going from 300 to 150 K. It is unlikely that reaction {48} can account for the relatively high temperatures seen in VertiCOIL.

As the models seem to be unable to account for the heat release, the Kirtland group is carefully re-evaluating their temperature measurements. The temperatures were determined from the lineshape of the I*-I 3-4 transition[5]. This line was observed using the absorption of light from a tunable diode laser. Turbulence in the gas flow near the walls and observation ports could influence the measurements and lead to overestimation of the temperature.

4. Mechanism of I_2 dissociation in COIL systems

The mechanism by which $O_2(a)$ dissociates I_2 in COIL systems is a long-standing unsolved problem[6]. This is an important issue as the dissociation process significantly impacts the efficiency of the laser. There are two mechanisms by which this occurs. First, as it takes an average of 4 to 6 $O_2(a)$ molecules to dissociate one I_2 molecule, the dissociation process consumes an appreciable amount of energy. Second, the time scale of the dissociation process influences energy extraction as it determines the downstream position at which the maximum concentration of I* will occur. The efficiency and time scale of the dissociation process depend on concentration ratios, mixing dynamics and total pressure. At present our ability to design new types of mixing nozzles and/or develop systems that operate at higher pressures is limited, in part, by our poor understanding of the dissociation kinetics.

The currently accepted model for I_2 dissociation is derived from flow tube studies conducted by Heidner et al.[21] These investigators were unable to find a unique kinetic model to account for their data. They offered two limiting models that defined a range of rate constants for the elementary reaction steps. The rate constant package used to predict COIL performance is mostly based on one of the limiting models[19,20]. The mechanism for I_2 dissociation assumes that vibrationally excited $I_2(X)$ is the immediate precursor of atomic Iodine[19,20]. However, subsequent measurements of $I_2(X)$ vibrational relaxation rate constants yielded values that were not in agreement with the rate constants used in COIL models[6,22].

As there is appreciable flexibility in the kinetic model, we considered the possibility that improvements could be made by constraining the vibrational relaxation rate constants and treating some of the less well known rate constants as variable parameters[7]. The original flow tube data of Heidner et al.[21] were used in this re-optimization procedure. This exercise was carried out in collaboration with Capt. J. S. Paschkewitz (Computational Sciences Branch, Air Vehicles Directorate, AFRL, Wright Patterson AFB). Improved rate constants were obtained that are significantly different from those used in current computational models. Unfortunately, although the new rate constants provided a better representation of the experimental data, troubling discrepancies remained. To make further progress we examined the possible participation of electronically excited states of I_2 (denoted by $I_2(A',A)$)[8]. Channels involving $I_2(A',A)$ were added to the standard COIL model and attempts were made to re-optimize the rate constant package by fitting the I_2 dissociation rate data. In the initial study the rate constant for the reaction

---

[a] In sections 1 and 2 the numbering of reactions is chosen to be consistent with the COIL standard rate constant package[19,20]. The number for each reaction is given in curly brackets.

$$I_2(X, v>20) + O_2(a^1\Delta) \rightarrow 2I + O_2(X^3\Sigma^-) \quad \{34\}$$

was not reduced below $k_{34}=1.5x10^{-11}$ cm^3 s^{-1} (1/20 the value used in the standard package). With such rapid dissociation of $I_2(X, v>20)$ the channel through the electronically excited states could not make a significant contribution. Preliminary indications were that the deficiencies of the standard model could not be overcome by including the participation electronically excited I_2[7]. However, restricting the range of values considered for k_{34} was somewhat arbitrary as there are no experimental data for this reaction. Greater reduction of k_{34} forces the dissociation process to proceed via electronic excitation of I_2. Under these conditions the kinetics become sensitive to electronic quenching of $I_2(A',A)$. A model of this form has the potential to give a good representation of the dissociation rate data, provided that quenching by Ar is very slow and that H_2O is more effective than $O_2(X)$ in dissipating energy from $I_2(A',A)$. It is probable that both the A' and A states of I_2 exhibit similar quenching kinetics. Hence, for simplicity the remainder of this discussion is focused on $I_2(A')$ (in addition, this species is appreciably more metastable than $I_2(A)$). Tellinghuisen and Phillips[23] have shown that quenching of $I_2(A')$ by Ar is slow ($k=2.8x10^{-14}$ cm^3 s^{-1}) and that the primary mechanism is collision induced dissociation. This seemed encouraging, but data for quenching by $O_2(X)$ and H_2O were needed to further examine the role of $I_2(A')$ in the dissociation process.

As the required rate constants for quenching of $I_2(A')$ by O_2 and H_2O were not available we measured these parameters using pulsed laser pump-probe techniques[24]. To populate the A' state a mixture of I_2 in Ar was excited by 193 nm pulses from an ArF laser. This initially promotes I_2 to the $D(0_u^+)$ state. Collisions with Ar rapidly induce transfer to the $D(2_g)$ state, which then radiates down to $A'^3\Pi(2_u)$. This sequence occurs within the radiative lifetimes of the D and D' states (approximately 10 ns). The population in the A' state was monitored by probe laser excitation of the $D'\leftarrow A'$ transition. Loss of population from A' was followed by varying the delay between the pump and probe lasers. For low concentrations of I_2 in 20 Torr of pure Ar the A' state decayed with a lifetime of about 30 μs. This was consistent with the earlier study by Tellinghuisen and Phillips[23]. Metered quantities of O_2 or H_2O were added to the I_2/Ar mixtures to observe quenching by these collision partners. The quenching rate constants were found to be $(6.3\pm0.6)x10^{-12}$ and $(3.4\pm0.4)x10^{-12}$ cm^3 s^{-1} for $O_2(X)$ and H_2O, respectively.

These measurements showed that both O_2 and H_2O are much more effective quenchers of $I_2(A')$ than Ar. However, Heidner et al.'s[21] models require H_2O to be a better deactivator than O_2 whereas the present results indicate the opposite trend. This apparent

disagreement can be resolved if quenching by O_2 is dominated by the Franck-Condon favored transfer process

$$I_2(A') + O_2(X^3\Sigma^-) \rightarrow I_2(X, v>10) + O_2(a^1\Delta) \quad \{28\}$$

Data for matrix isolated I_2/O_2 mixtures shows that this is, indeed, a facile transfer process[25].

To test the notion that $I_2(A')$ is a significant dissociation intermediate, a new kinetic model of the dissociation process has been examined[24]. This model, which is shown schematically in Fig. 5, is based on the standard reaction set with the addition of reactions involving $I_2(X, 10<v<20)$ and $I_2(A')$. The full set of reactions and rate constants is listed in Table 1. Numerical integration of the coupled rate equations was used to predict $I_2(X)$ removal kinetics. Several rate constants were manually adjusted to achieve reasonable agreement with the dissociation rate data of Heidner et al.[21] The revised model gives a significantly better fit to the experimental data than the standard package. From a chemical physics perspective the most appealing aspect of the model is that the rate constants all have magnitudes that are appropriate for the types of process that they are associated with. Note that the specific values for the rate constants in Table 1 are not unique and they are not fully optimized. Improvements could be achieved by coupling the differential equation solver with a non-linear least squares fitting routine.

The ability of this new model to predict the performance of COIL systems is being tested by Dr. T. Madden (AFRL Kirtland) and Dr. B. Barmashenko (Ben Gurion University, Israel). Preliminary results from the group at BGU indicate that the model gives much improved predictions for the dependence of the laser power on the reagent concentrations and flow conditions.

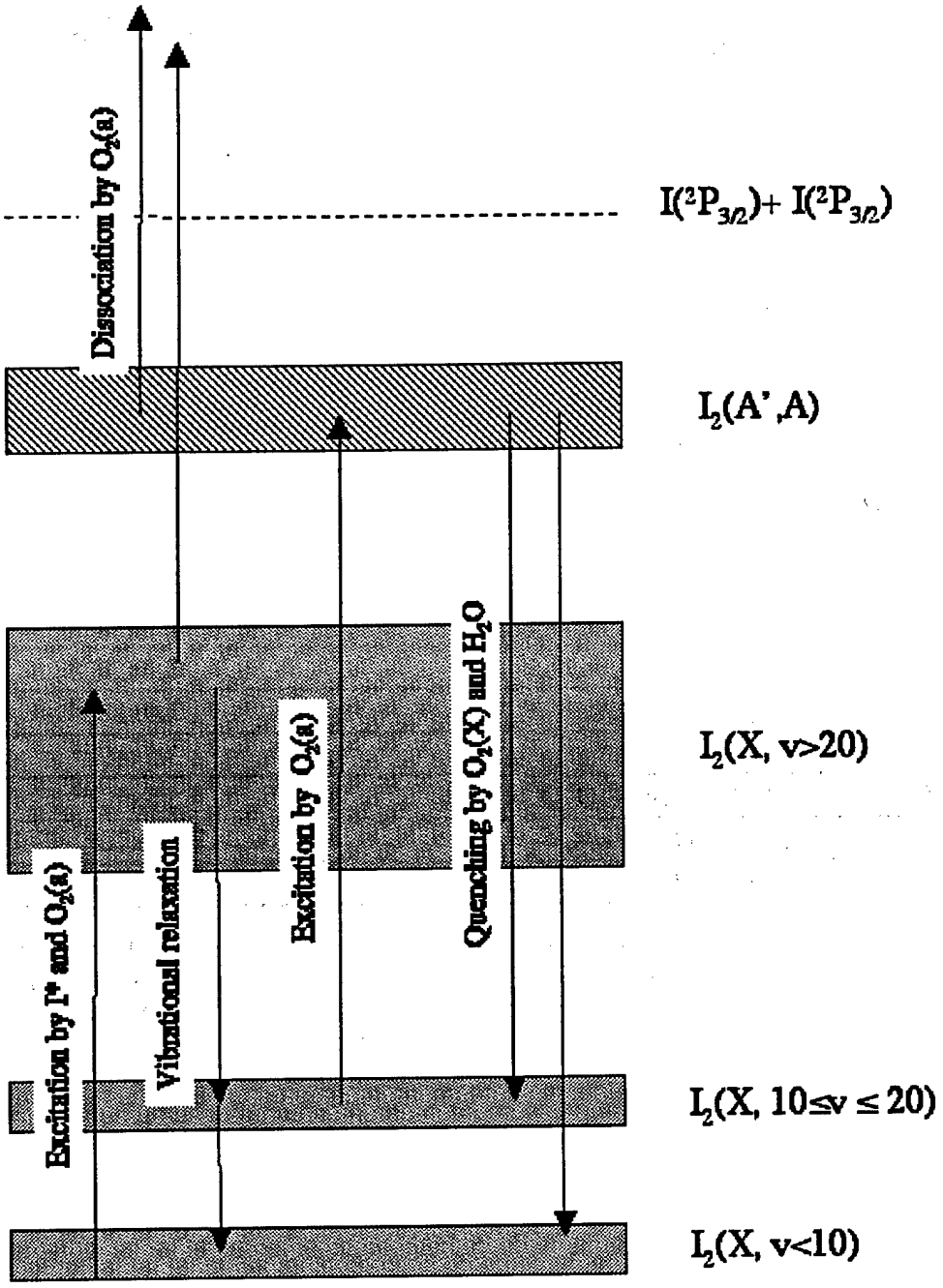

Figure 5. Schematic of the proposed dissociation mechanism

Table 1. Kinetic scheme used to simulate the experimental data of Heidner et al.[21]

Reaction #	Reaction	Rate Constant/ cm^3 s^{-1}
1	$O_2(a)+O_2(a)\rightarrow O_2(b)+O_2(X)$	$2.7x10^{-17}$
21	$O_2(b)+I_2\rightarrow O_2(X)+2I$	$4.0x10^{-12}$
40	$O_2(a)+I\rightarrow O_2(X)+I^*$	$7.6x10^{-11}$
41	$O_2(X)+I^*\rightarrow O_2(a)+I$	$2.6x10^{-11}$
44	$O_2(a)+I^*\rightarrow O_2(b)+I$	$1.1x10^{-13}$
32	$O_2(a)+I_2\rightarrow O_2(X)+I_2^{**}$	$\mathbf{2.0x10^{-14}}$
34	$O_2(a)+I_2^{**}\rightarrow O_2(X)+2I$	$\mathbf{1x10^{-13}}$
27	$\mathbf{O_2(X)+I_2^{**}\rightarrow O_2(X)+I_2^*}$	$\mathbf{3x10^{-12}}$
39	$\mathbf{H_2O+I_2^{**}\rightarrow H_2O+I_2^*}$	$\mathbf{5x10^{-12}}$
38	$\mathbf{I_2^*+O_2(a)\rightarrow I_2(A')+O_2(X)}$	$\mathbf{6x10^{-12}}$
25	$I_2(A')+O_2(a)\rightarrow 2I+O_2(X)$	$\mathbf{2x10^{-10}}$
28	$\mathbf{I_2(A')+O_2(X)\rightarrow I_2^*+O_2(a)}$	$\mathbf{6.3x10^{-12}}$
29	$\mathbf{I_2(A')+H_2O\rightarrow I_2+H_2O}$	$\mathbf{3.4x10^{-12}}$
63	$\mathbf{I_2^*+H_2O\rightarrow I_2+H_2O}$	$\mathbf{1.2x10^{-12}}$
64	$\mathbf{I_2^*+O_2(X)\rightarrow I_2+O_2(X)}$	$\mathbf{1.5x10^{-12}}$
65	$\mathbf{I_2^{**}+Ar\rightarrow I_2^*+Ar}$	$\mathbf{2.0x10^{-12}}$
66	$\mathbf{I_2^*+Ar\rightarrow I_2+Ar}$	$\mathbf{2.0x10^{-13}}$
33	$I^*+I_2\rightarrow I+I_2^{**}$	$3.5x10^{-11}$
5	$O_2(b)+H_2O\rightarrow O_2(X)+H_2O$	$5.5x10^{-12}$
48	$I^*+H_2O\rightarrow I+H_2O$	$2.0x10^{-12}$
67	$\mathbf{O_2(b)+I_2^*\rightarrow O_2(X)+2I}$	$\mathbf{3.0x10^{-12}}$

Boldface type is used to indicate reactions that are not part of the standard package and rate constants that have been assigned values that are different to those used in the standard package. The reaction numbering scheme is chosen to be consistent with Table 1 of reference [20] I_2^{**} is $I_2(X,v>20)$ and I_2^* is $I_2(X, 10\leq v<20)$.

5. Kinetic Studies of the NCl radical.

5a. Quenching rate constants for NCl(a)

Interest in the possibility of using NCl(a) as the energy carrier in iodine laser systems[9-11] motivated several previous studies of NCl(a) removal kinetics[12-14]. Two different experimental techniques were used to determine quenching rate constants, and the results appeared to be strongly dependent on the technique used. Hewett et al.[14] performed measurements in a discharge flow system. NCl(a) was generated from the reaction

$$Cl + N_3 \rightarrow NCl(a) + N_2 \qquad (5)$$

and the intensity of the NCl a-X system was monitored as a function of quenching gas density and time under steady state conditions. Alternatively, Ray and Coombe[12], and Henshaw et al.[13] used pulsed photolysis of ClN_3 to generate NCl(a), and time-resolved fluorescence measurements to determine quenching rate constants. As photolysis of ClN_3 produces strong emissions from the N_2 B-A system, an interference filter was used to isolate the NCl a-X fluorescence. Ray and Coombe[12] reported that NCl(a) generated by 248 nm photolysis of ClN_3 has a complex time profile. Under certain conditions they found that the NCl(a) signal could show rise-fall characteristics. This behavior was attributed to secondary generation of NCl(a) from chain decomposition of ClN_3. Chain decomposition did not appear to be of importance when 193 nm photolysis was used. Instead, bi-exponential decays were observed. The long-lived component of the decay was attributed to NCl(a). Ray and Coombe[12], and Henshaw et al.[13] (who also used 193 nm photolysis) determined NCl(a) removal rate constants by observing the dependence of the long-lived decay rate on the pressure of added quenchers or reactants. The level of agreement between the rate constants reported by these two groups was good, but several of the constants were dramatically different from values measured in a discharge flow system by Hewett et al.[14] We re-examined the photolysis approach to probe the origin of these discrepancies and determine which data are most reliable.

In our experiments NCl(a) was generated by photolysis of ClN_3. The apparatus used for these measurements is shown in Fig. 6. The generator used to provide ClN_3 was the same as that described by Henshaw et al.[13] The azide was formed when a mixture of 5% Cl_2 in He was passed over the surface of moist NaN_3. A standard drying agent was used to remove water from the ClN_3/Cl_2/He mixture at the exit of the generator. The concentration of ClN_3 was monitored via the absorption band at 250 nm. After the generator had been run for a few hours, the efficiency for converting Cl_2 to ClN_3 was typically 85-95%. Due to incomplete conversion, a background concentration of Cl_2 was always present in the photolysis cell.

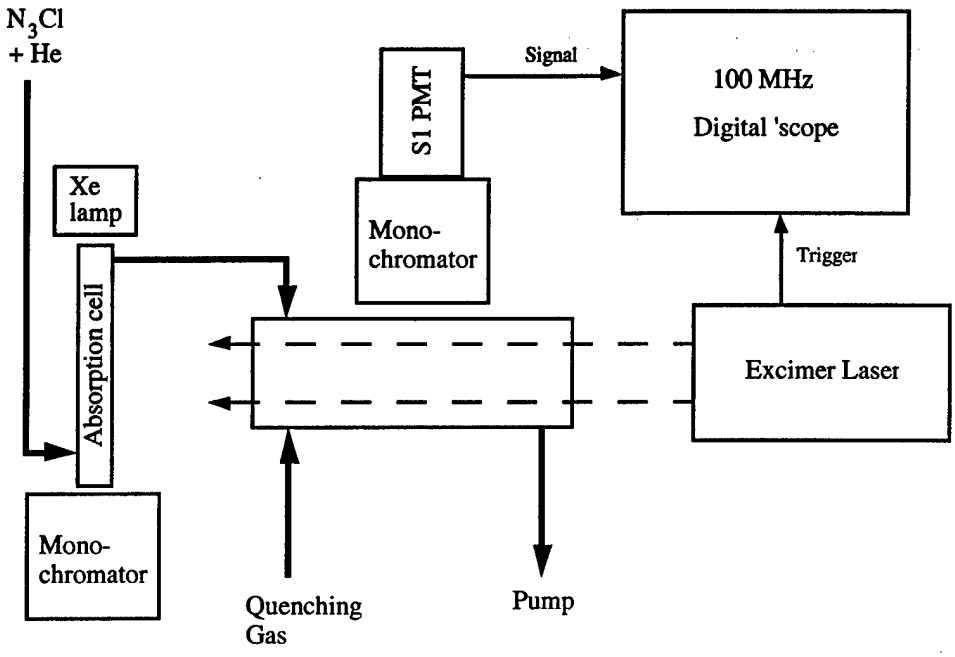

Figure 6. Apparatus used to observe the fluorescence decay and quenching of NCl(*a*).

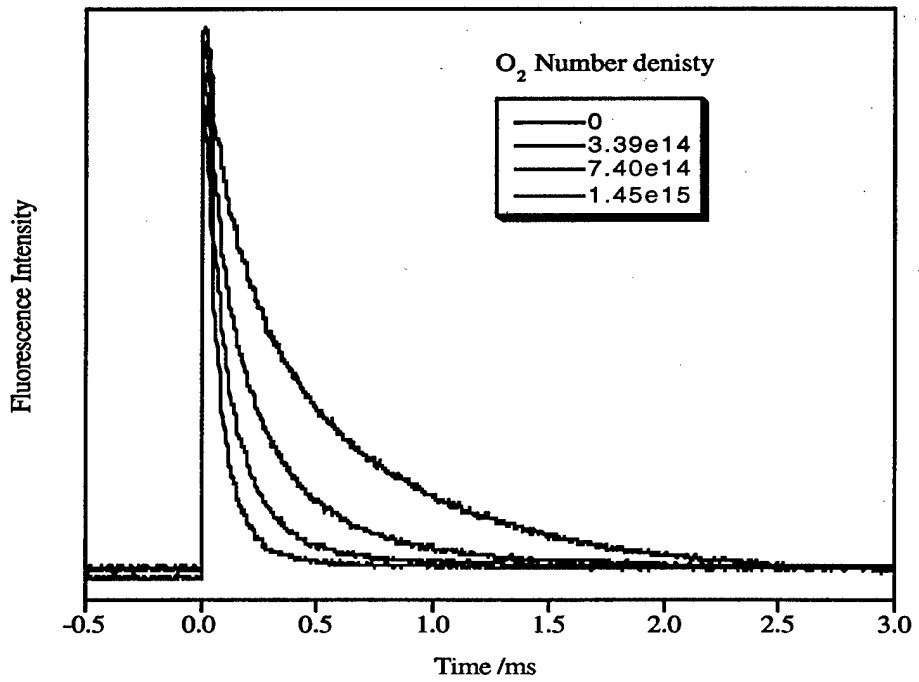

Figure 7. Fluorescence decay curves for NCl(*a*) in the presence of O_2

Low photolysis laser powers were used to photodisociate the ClN_3 for the NCl(a) quenching rate constant measurements. Emissions resulting from photolysis were dispersed by a 0.2 m monochromator. For detection of fluorescence with λ>700 nm, a 695 nm long-pass filter was placed between the photolysis cell and the monochromator to block scattered laser light and short wavelength emission signals. The dispersed light was detected by a cooled photomultiplier tube (Hamamatsu R1767, S1 photocathode). To record emission spectra, the output from the phototube was processed by a boxcar integrator (SRS 250). The time dependence of the fluorescence signals was examined using a digital storage oscilloscope (LeCroy ScopeStation 140, 100MHz bandwidth). Signal averaging was used to improve the signal to noise ratios.

For 193 nm photolysis of ClN_3 we found that the emission spectrum in the vicinity of the NCl a-X 0-0 band was very congested. The interfering emissions included strong bands from the N_2 B-A system. Attempts to determine NCl(a) removal rate constants using 193 nm photolysis produced very scattered results. Surprisingly, we found that 248 nm photolysis produced an emission spectrum dominated by the NCl a-X 0-0 band. The time dependence of this emission gave a good fit to a single exponential decay. Our initial observations were made using the unfocused output from an excimer laser, which provided fluences of the order of 30 mJ cm^{-2} in the cell. The extent of chain decomposition should be dependent on the laser power, and may be insignificant when low fluences are used. However, when the laser was focused by a 1 m focal length lens we were still unable to observe temporal profiles that showed evidence of secondary NCl(a) production.

As 248 nm photolysis appeared to be suitable for kinetic measurements in our apparatus, we examined removal of NCl(a) by O_2, Cl_2, HCl, and H_2[15]. Typical fluorescence decay curves for various pressures of O_2 are shown in Fig. 7. Stern-Volmer plots for removal by O_2, Cl_2, and HCl are shown in Fig. 8. Quenching rate constants determined in the present study are collected in Table 2, where they may be compared with the results of previous measurements. The rate constant for quenching by O_2 was greater than previous values by a factor of two. However, the higher value was supported by the time-resolved data for NCl(X) (described below). The rate constants for removal by Cl_2, HCl, and H_2 were much closer to the flow tube results[14] than the values obtained using 193 nm photolysis[12,13]. At present we do not know the reason for the large discrepancy between the results of Hewett et al.[14] and those of Ray and Coombe[12], and Henshaw et al.[13]

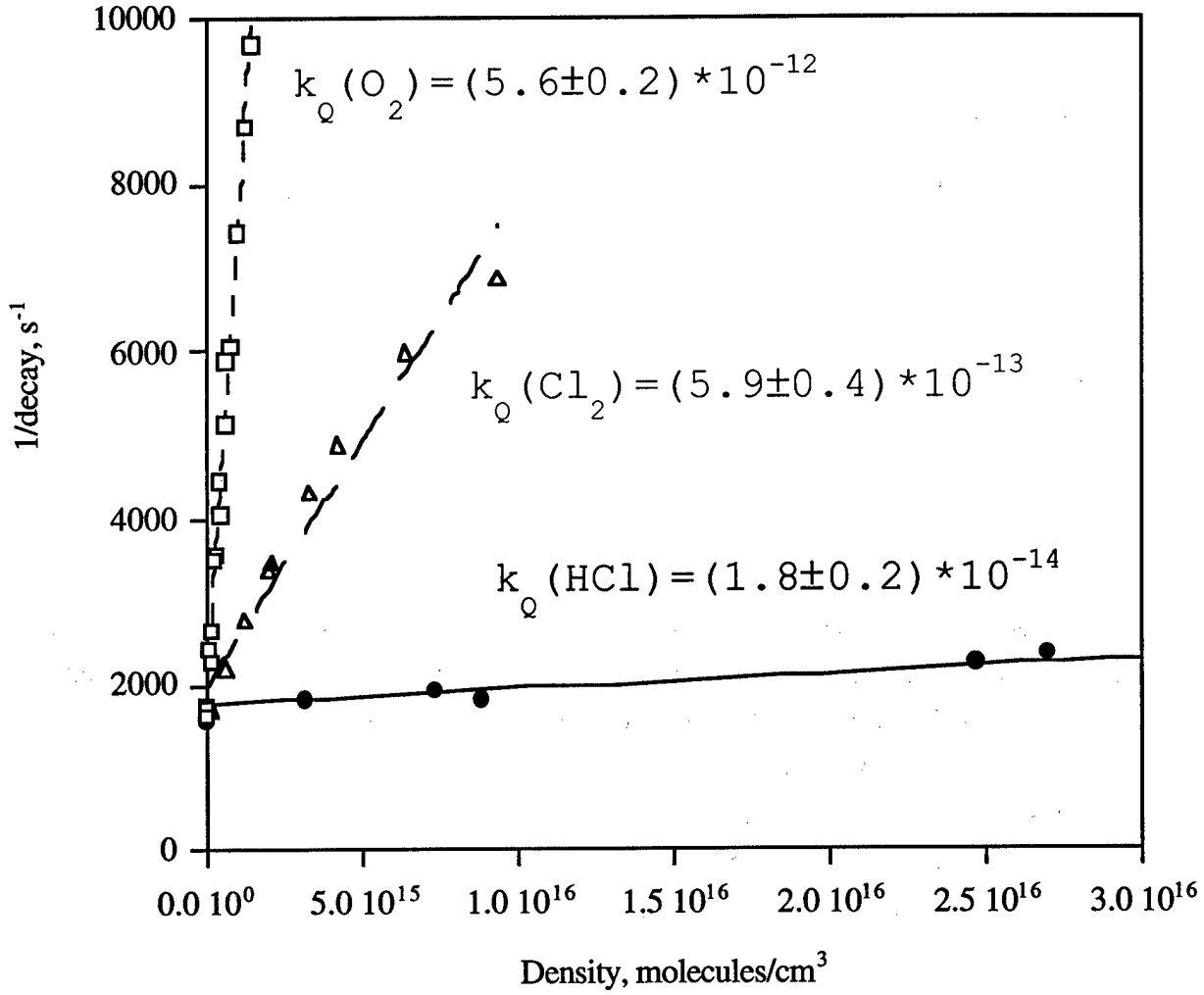

Figure 8. Stern-Volmer plots for quenching of NCl(a) by O_2, Cl_2, and HCl.

Table 1

Comparison of Rate Constants for Removal of NCl(a)

Collision partner	Rate Constant /10^{-14} cm^3 s^{-1}			
	1	2	3	4
O_2	560±40	280±60	250±20	--
Cl_2	59±8	40±10	1800±300	2900±600
HCl	1.8±0.4	1.5±0.3	490±70	--
H_2	<0.1	<0.1	68±7	--
N_3Cl	30±10	--	--	57±4

1. Present work
2. K. B. Hewett, G. C. Manke, D. W. Setser, and G. Brewood, *J. Phys. Chem. A,* **104,** 539-551 (2000).
3. A. J. Ray and R. D. Coombe, *J. Phys. Chem.* **98**, 8940 (1994)
4. T. L. Henshaw, S. D. Herrera, G. W. Haggquist, L. A. Schlie, *J. Phys. Chem. A.* **101**, 4048 (1997).

5b. Removal of NCl(a) by I_2.

Quenching of NCl(a) by I_2 is described separately, as the characteristics of this process were somewhat different to those of the quenching agents described above. Stern-Volmer plots for NCl(a)+I_2 were linear, but the slopes were dependent on the repetition frequency of the photolysis laser. The apparent quenching rate constant increased from around $6x10^{-11}$ cm^3 s^{-1} at 10 Hz to $1.0x10^{-10}$ at 0.5 Hz. Further increases in the rate constant did not occur for repetition rates slower than 0.5 Hz. These data indicated that NCl(a) was being removed by reaction with I_2, and that the gas sample was not being fully replenished between laser shots for repetition frequencies above 0.5 Hz. To avoid this problem, measurements on the ClN_3/I_2 system were carried out using a pulse repetition frequency of 0.2 Hz. Under these conditions the removal rate constant for I_2 was $(1.0\pm0.3)x10^{-10}$ cm^3 s^{-1}. Note that the rate constant at 10 Hz was still relatively large, which suggests that NCl(a) is efficiently quenched by one or more of the reaction products.

To test the hypothesis that NCl(a) was being removed by a reactive process, we monitored the time-dependent behavior of I_2 following photolysis of $He/I_2/ClN_3$ mixtures. Fig. 9 shows the apparatus used for these measurements. The 488 nm radiation from an Ar ion laser was used to monitor I_2 via the *B-X* continuum absorption. An advantage of this approach is that the strength of the absorption signal is insensitive to vibrational excitation of $I_2(X)$. The time dependent behavior of the absorption signal is shown by trace (a) in Fig. 10. The initial negative-going spike (0-200 μs) in this trace was caused by radio frequency noise from the pulsed laser. The absorption signal recovered with a time constant of about 340 s^{-1}. This was consistent with diffusion of I_2 into the photolysis region from the surrounding un-irradiated gas. Trace (b) was recorded with just an I_2/He mixture present in the cell. This measurement, which shows only the initial noise spike, was made to demonstrate that I_2 was not being dissociated by the 248 nm pulse.

Photolysis of $He/ClN_3/I_2$ mixtures yielded emission from I*. Fig. 11a shows the time dependence of the I* signal for various initial I_2 pressures. Note that I* signals were not observed for 248 nm excitation of flowing mixtures of He/I_2 or $He/Cl_2/I_2$. The finite rise time of the I* signal for photolysis of $He/ClN_3/I_2$ mixtures indicated that I* was being generated by secondary photochemical reactions. Given that NCl(a) reacts with I_2 it is probable that I* was generated by the sequence

$$ClN_3 + h\nu \rightarrow NCl(a) + N_2 \quad (6)$$

$$NCl(a) + I_2 \rightarrow INCl + I \quad (7)$$

$$NCl(a) + I \rightarrow NCl(X) + I^* \quad (8)$$

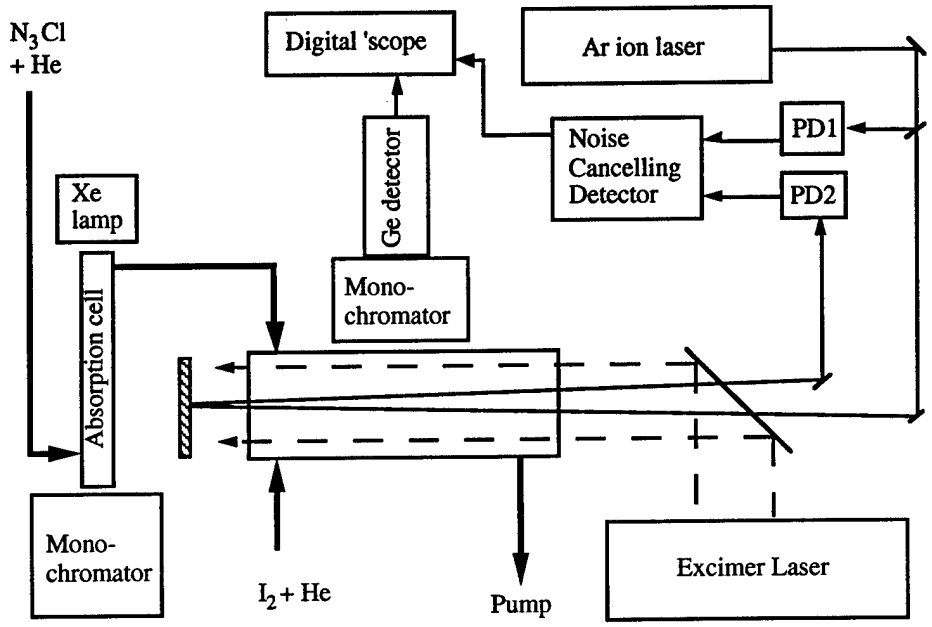

Figure 9. Apparatus used to observe I_2 and I* kinetics following photolysis of $He/ClN_3/I_2$ mixtures.

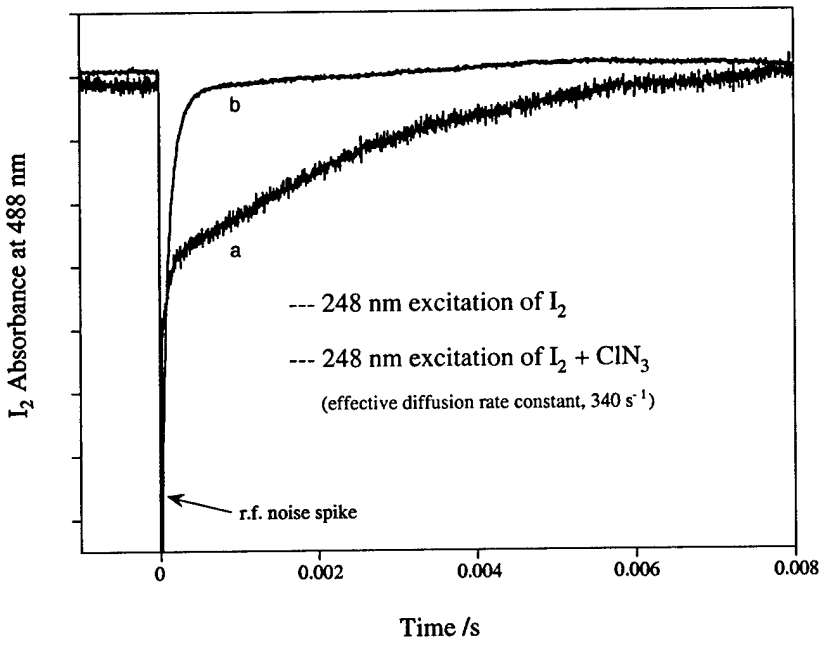

Figure 10. Removal of I_2 by NCl(a)

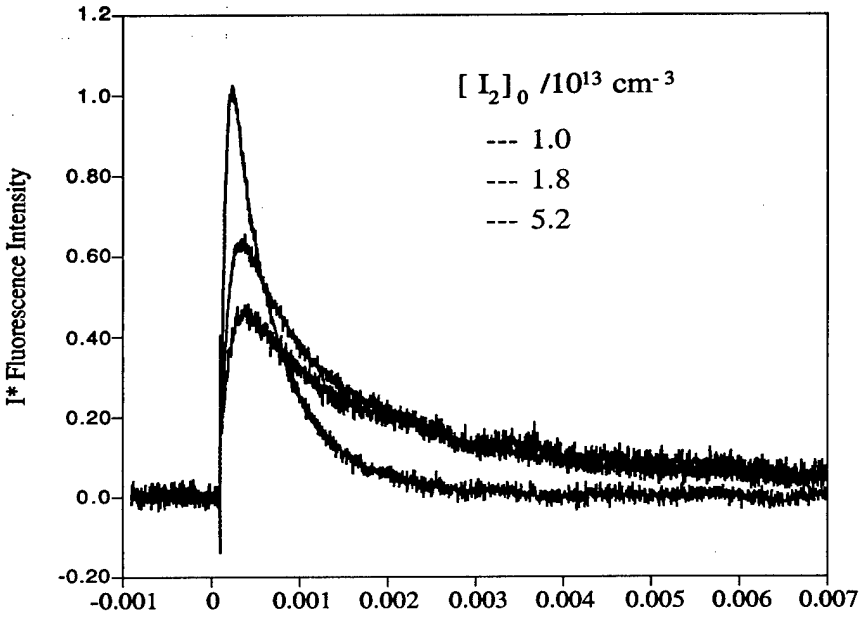

Figure 11a. I* emission following photolysis of $He/ClN_3/I_2$ mixtures

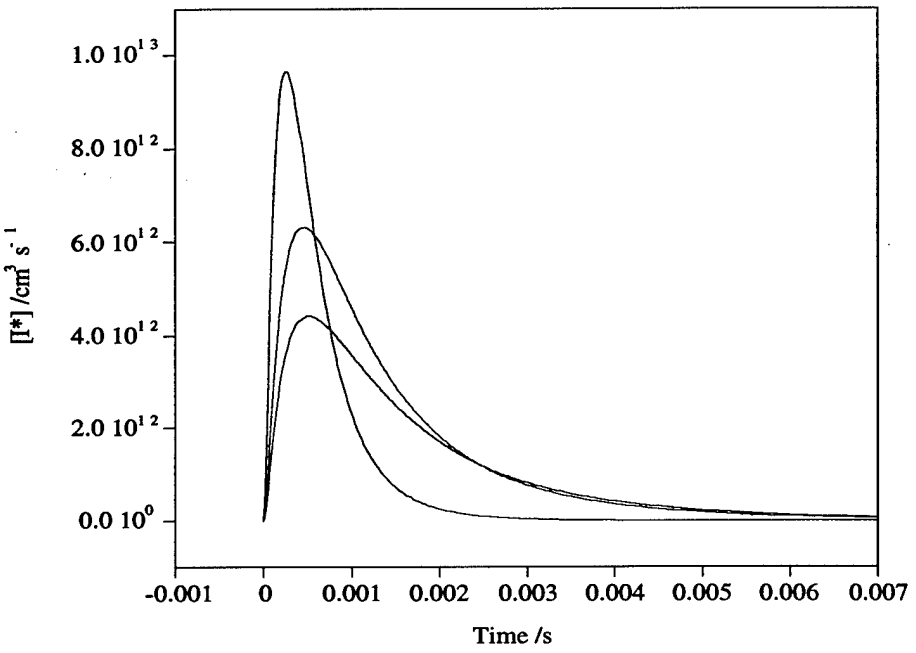

Figure 11b. Kinetic simulations of the curves shown in Fig. 11a. See text for details.

We simulated the I* temporal profiles using a kinetic model that included the above reactions (6, 7, and 8) and the additional processes

$$NCl(a) + ClN_3 \rightarrow \text{products} \quad (9a)$$

$$NCl(a) + ClN_3 \rightarrow NCl(X) + ClN_3 \quad (9b)$$

$$NCl(a) + Cl_2 \rightarrow NCl_2 + Cl \quad (10)$$

$$I^* + I_2 \rightarrow I + I_2 \quad \{33\}$$

$$I^* + ClN_3 \rightarrow \text{products} \quad (11)$$

$$I^* + INCl \rightarrow I + INCl \quad (12)$$

$$NCl(a) + INCl \rightarrow NCl(X) + INCl \quad (13)$$

Literature values were available for the rate constants needed for this model with the exception of the constants for reactions 12 and 13. However, attempts to simulate the I* kinetics (Fig 11a) were unsuccessful regardless of the values chosen for k_{12} and k_{13}. The problem was traced to the quenching of I* by ClN_3, which proceeded much too rapidly in the model. To obtain agreement with the experimental data the rate constant for reaction 11 had to be reduced to values below $2x10^{-14}$ cm^3 s^{-1}. The model also required relatively large rate constants for quenching of I* and NCl(*a*) by the product(s) of reaction 7. The best simulation, which is shown in Fig. 11b, was obtained using $k_{12}=4x10^{-11}$ and $k_{13}=2.5x10^{-11}$ cm^3 s^{-1}.

In the above model we have tentatively assumed that the reaction of NCl(*a*) with I_2 gives INCl as a product. This is analogous to the reaction between NCl(*a*) and Cl_2. To date there have been no reported observations of INCl, but ab initio calculations predict that this radical is bound by at least 1 eV.

5c. Detection and characterization of NCl(X) via b-X absorption spectroscopy (collaboration with Dr. G. C. Manke II (AFRL, NM) and Dr. S. J. Davis(PSI, MA)).

A method for detecting NCl(*X*) via the *b-X* absorption bands was developed for three reasons. First, the *b-X* bands provide a convenient diagnostic for the conditions within an NCl/I laser system. High-resolution absorption measurements can provide local temperature and concentration information. Second, time-resolved monitoring of NCl(*X*) in kinetics experiments can be used to learn more about the collision dynamics of both NCl(*X*) and NCl(*a*). Third, monitoring of NCl(*X*) was used to examine the NCl(*a*)/NCl(*X*) ratio produced by photolysis of ClN_3.

The apparatus used to observe the NCl(*X*) absorption spectra is shown in Fig. 12. NCl was generated by photolysis of ClN_3 (at 193 or 248 nm). The output from a CW ring dye laser was used to observe the *b-X* bands near 665 nm.

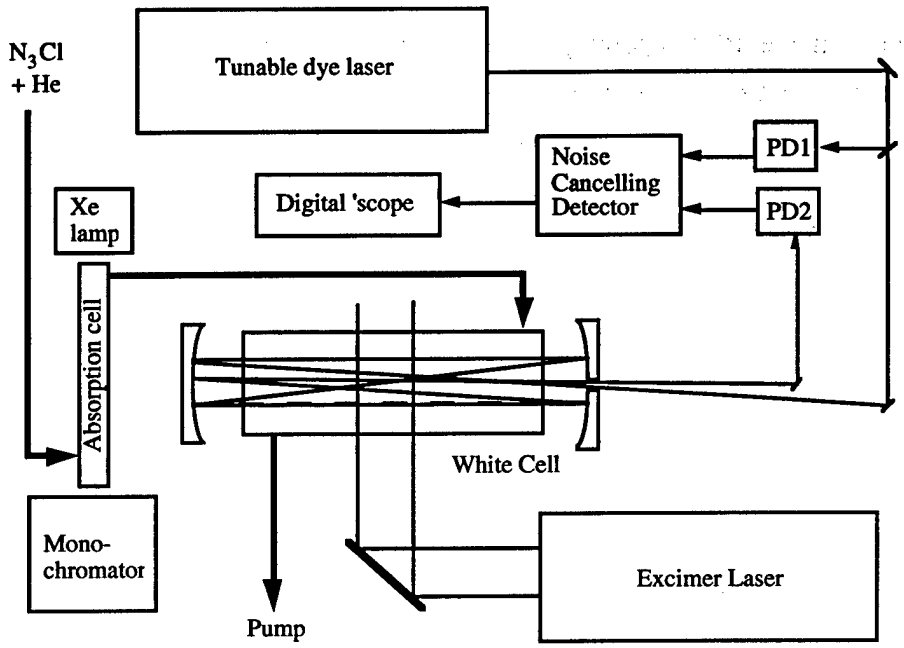

Figure 12. Apparatus used to observe the NCl *b-X* absorption bands.

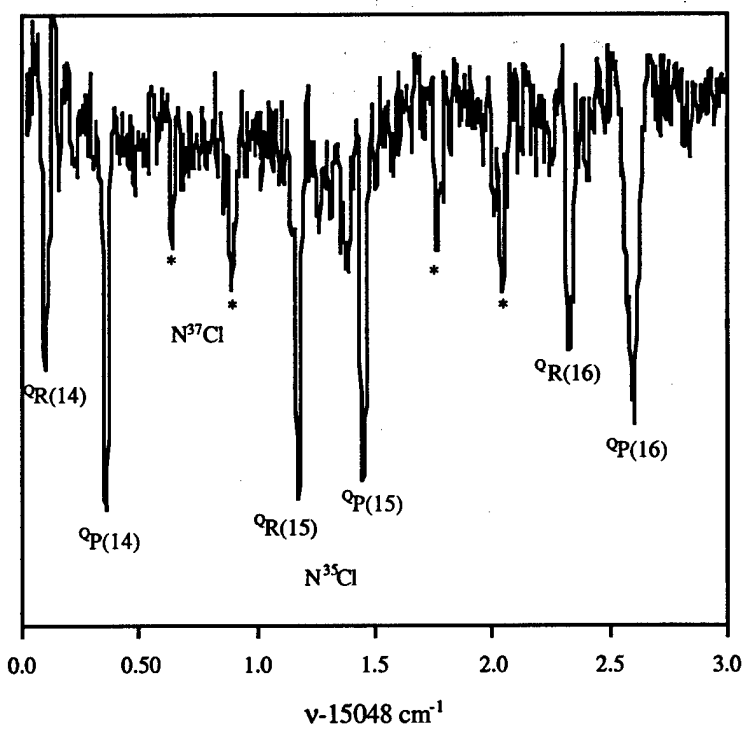

Figure 13. Section of the NCl b-X absorption spectrum

The beam was split into reference and sample beams. White cell mirrors were used to obtain about 100 passes of the sample beam through the absorption cell. The sample and reference beams were then processed by a noise canceling detector system (New Focus Nirvana detector).

A typical NCl absorption spectrum from this apparatus is shown in Fig. 13. Note that the signal-to-noise ratio of this trace was limited by the scanning electronics that control the dye laser. The minimum sweep speed was not slow enough to permit extensive signal averaging. The relative positions of the *b*-*X* 0-0 band rotational lines were in excellent agreement with the work of Colin and Jones[26]. However, we found a small systematic calibration error in the former study. Our measurements indicate that the line positions of Colin and Jones should be reduced by 0.04 cm^{-1}. This correction is of significance for the development of diode laser diagnostic instruments. Fig. 13 and similar spectra were recorded in the presence of 6 Torr of buffer gas (mostly He), with a 100 μs delay between the photolysis pulse and the absorption measurement (a boxcar integrator was used to monitor absorption after a fixed delay). Under these conditions the rotational and translational energy of NCl should be in thermal equilibrium with the buffer gas. This was confirmed by the rotational line intensity distribution, which defined a rotational temperature of 300±20 K. The translational temperature was estimated from absorption line profiles. The lineshapes were well represented by a Gaussian function with a linewidth of 0.031 cm^{-1} (FWHM). This is slightly wider than would be expected for a temperature of 300 K (predicted width of 0.026 cm^{-1}). However, fitting to a single Gaussian function ignores the hyperfine structure of the ro-vibronic transitions. We have calculated the hyperfine structure of the line, and found that the transitions span a range of 0.05 cm^{-1}. Convolution of the hyperfine structure with the Doppler lineshape for 300 K readily accounts for the observed linewidth. Clearly, diagnostic techniques that use the profiles of NCl rotational lines for temperature determination will need to take the hyperfine structure of the lines into account.

Searches were made for transitions originating from vibrationally excited levels of NCl(*X*), to examine the possibility that vibrationally excited products are produced by photolysis of ClN_3. We were unable to detect population in the v=1 or 2 levels using either 193 or 248 nm photolysis. From these measurements, and estimates of the sensitivity of the apparatus, we conclude that 60% or more of the NCl(*X*) is produced in the v=0 level.

The primary product resulting from UV photolysis of ClN_3 is NCl(*a*). Previous studies[27] have shown that O_2 quenches NCl(*a*) by the E-E transfer process

$$NCl(a) + O_2(X) \rightarrow NCl(X) + O_2(a) \qquad (14)$$

In the absorption measurements, addition of O_2 to the photolysis cell produced an increase in the NCl(X) concentration. For example, Fig. 14 shows scans over the $^QP(14)$ line with and without O_2 present in the photolysis cell. These traces were recorded using 193 nm photolysis light. The dependence of the NCl(X) signal on O_2 pressure was consistent with a competition between quenching and removal of NCl(a) by processes that do not generate NCl(X) (e.g., NCl(a)+$ClN_3 \rightarrow NCl_2 + N_3$). For O_2 partial pressures above 0.5 Torr the NCl(X) signal was not perceptibly dependent on further addition of O_2, indicating that NCl(a) removal was dominated by O_2 quenching under these conditions. If it is assumed that all of the NCl(a) created by photolysis is quenched by O_2 at the high pressure limit, data such as those shown in Fig. 14 yield a branching fraction for N_3Cl + 193 nm $\rightarrow$ NCl(a) + N_2 of approximately 0.75. Similar measurements performed using 248 nm photolysis indicate that the branching fraction for N_3Cl + 248 nm $\rightarrow$ NCl(a) + N_2 is greater than 0.8.

Fig. 15 shows a typical time-resolved absorption signal. Such data were recorded for a variety of total pressures and added quenching gas conditions. The results were analyzed by kinetic modeling. For example, the data for energy transfer induced by O_2 were analyzed by a model based on the reactions

$$ClN_3 + 248 \text{ nm} \rightarrow NCl(a) + N_2 \quad (6)$$

$$NCl(a) + ClN_3 \rightarrow \text{products} \quad (9)$$

$$NCl(a) + Cl_2 \rightarrow NCl_2 + Cl \quad (10)$$

$$NCl(a) + O_2(X) \rightarrow NCl(X) + O_2(a) \quad (14)$$

$$NCl(X) + NCl(X) \rightarrow N_2 + 2Cl \quad (15)$$

$$NCl(X) + ClN_3 \rightarrow \text{products} \quad (16)$$

The rate constants for most of these reactions were determined from quenching studies (see Table 2). Clyne et al.[28] reported a rate constant of 8.1×10^{-12} cm^3 s^{-1} for reaction 15, and the pseudo first order removal of NCl(X) by ClN_3 was represented by a decay rate of 2800 s^{-1}. The smooth curve in Fig. 15 illustrates the ability of this kinetic model to fit the absorption data. Note that we have assumed a branching fraction for NCl(a) formation of one for this model. In earlier analyses of these data we did not include the NCl(X)+NCl(X) reaction[15]. Without this process the kinetic model was unable to reproduce the relatively fast rise times of the absorption signals. To account for the fast rise times we assumed that vibrationally excited NCl(X, v>0) was formed and rapidly relaxed by collisions with the buffer gas. With reaction 15 in the model this assumption was not required.

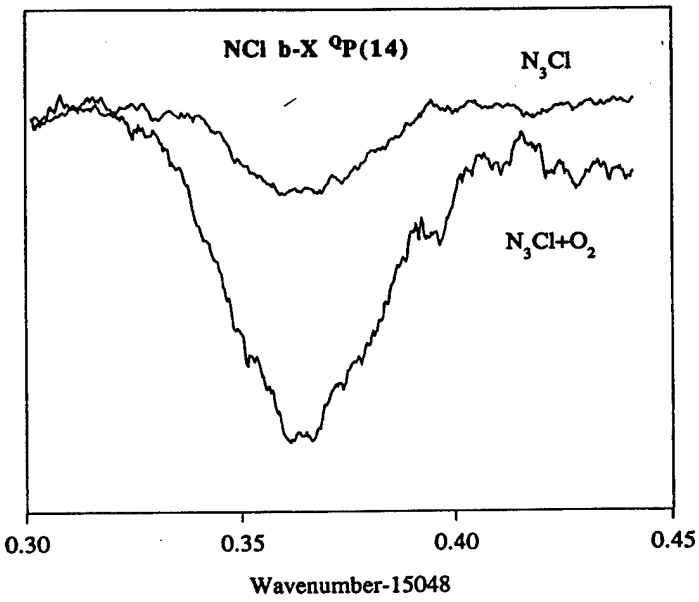

Figure 14. Scans over the NCl(X) ^{Q}P(14) line for photolysis of He/ClN_3 and He/ClN_3/O_2 mixtures.

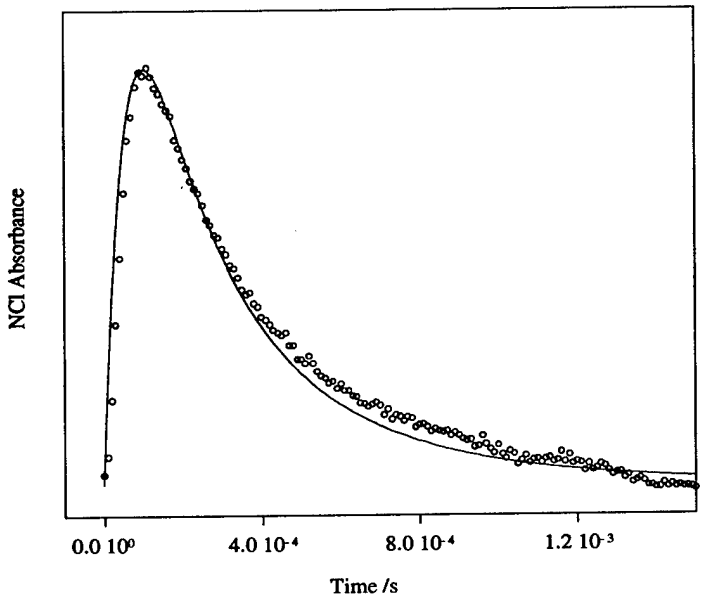

Figure 15. Time resolved absorption of NCl(*X*) from photolysis of ClN_3 in the presence of O_2 ($[O_2]=2.2x10^{15}$ cm^{-3}). The smooth curve shows a fit of the kinetic model to the data. See text for details..

5d. Determination of the NCl(a) self-annihilation rate constant

Self-annihilation of NCl(*a*),

$$NCl(a) + NCl(a) \rightarrow \text{products} \qquad (17)$$

is one of the most critical reactions for any laser that relies on this metastable as an energy carrier. The room temperature rate constant for NCl(*a*) self-annihilation was investigated by Henshaw et al.[13] who reported a value of $(7.2\pm0.9)\times10^{-12}$ cm^3 s^{-1}. However, our work on NCl(*a*) decay kinetics indicated that there may have been significant problems with this measurement[15]. Consequently, we re-examined NCl(*a*) self-annihilation.

The self-annihilation process cannot be observed under pseudo first-order conditions. To extract the rate constant from second order decay data, the absolute concentration of NCl(*a*) must be known. In the experiments described here we used 248 nm photolysis of ClN_3 to generate NCl(*a*). The absolute concentration was derived using the branching ratio for formation of NCl(*a*) established by the measurements described in the previous section.

Our studies of NCl(*a*) quenching kinetics were carried out using low photolysis laser fluences. Small concentrations of NCl(*a*) were formed, and the fluorescence decay curves showed no evidence of second order removal processes. The conditions of these experiments were such that initial NCl(*a*) densities of about 4×10^{14} cm^{-3} were generated. To achieve conditions where second order removal of NCl(*a*) could be observed we focused the beam from the photolysis laser to dissociate a larger fraction of the ClN_3. A 1m focal length lens was used to focus the beam, and neutral density filters were used to vary the power transmitted to the photolysis cell. Imaging optics were used to collect the fluorescence emitted from the focal volume. The fluorescence was dispersed by a 0.25 m monochromator and detected by a photomultiplier with an extended S1 photocathode.

Fig.'s 16 and 17 show NCl(*a*) fluorescence decay curves recorded for a range of laser powers. These traces were obtained with 7 Torr of the ClN_3/Cl_2/He mixture present in the photolysis cell. The ClN_3 absorption diagnostic indicated that >90% of the Cl_2 had been converted to ClN_3. The curves in Fig. 2 show an increase in the initial decay rate with increasing laser intensity. This behavior is readily understood using the kinetic model proposed by Henshaw et al.[13] Removal of NCl(*a*) can be considered in terms of the second order self-annihilation and an effective rate for all first-order loss processes (k_L), such that

$$-\frac{d[NCl(a)]}{dt} = k_{17}[NCl(a)]^2 + k_L[NCl(a)] \qquad (18)$$

where $k_L=k_9[ClN_3]+k_{11}[Cl_2]+k_D$, and k_D is the diffusion rate. From this expression it is apparent that the initial decay rate will depend on $[NCl(a)]_0$, which in turn depends on the

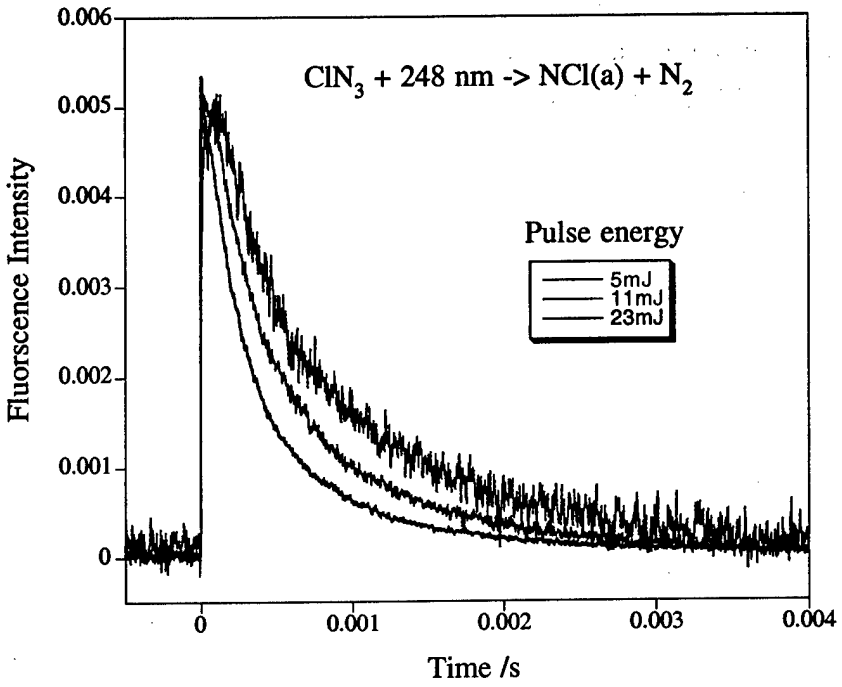

Figure 16. NCl(a) decay as a function of photolysis laser energy. These curves have been scaled to give comparable intensities.

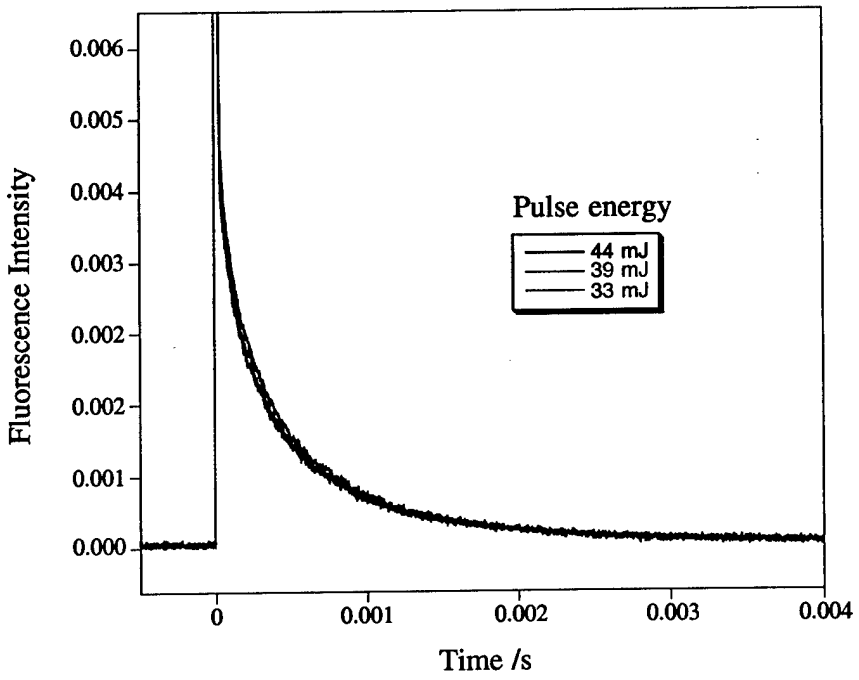

Figure 17. NCl(a) decay curves recorded using high photolysis laser intensities. These are unscaled curves. The signal intensities were not dependent on the laser pulse energy in this range.

laser intensity. Fig. 17 shows that, above a certain threshold, the NCl(a) decay curves became independent of laser intensity. We attribute this behavior to complete photolytic destruction of ClN_3. Once this threshold has been crossed the initial NCl(a) concentration is no longer dependent on the laser intensity. To check the validity of this interpretation we calculated the intensity needed to achieve complete dissociation from the ClN_3 absorption cross section[13] (1.5×10^{-18} cm^2 at 248 nm) and compared this with the observed threshold intensity. The theoretical threshold for complete dissociation (530 mJ cm^{-2}) was a little lower than the observed value (600 mJ cm^{-2}), but the agreement was reasonably good given that the window losses were not accurately characterized.

To determine the self-annihilation rate constant the decay curves recorded using high laser intensities (complete dissociation) were fit using the integrated form of Eq. 18,

$$[\mathrm{NCl}(a)] = \frac{k_L[\mathrm{NCl}(a)]_0}{\exp(k_L t)\left(k_{17}[\mathrm{NCl}(a)]_0 + k_L\right) - k_{17}[\mathrm{NCl}(a)]_0} \qquad (19)$$

The initial NCl(a) concentration was calculated by assuming 90% conversion of Cl_2 to ClN_3, and a branching fraction of 0.8 for generation of NCl(a) from ClN_3 photolysis. Fig. 18 shows an example of the level of agreement obtained between the data and the fitted curves.

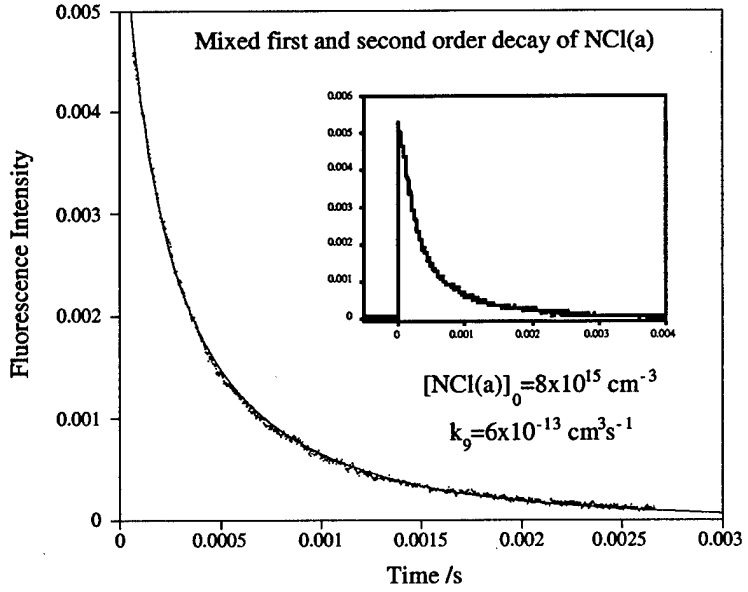

Figure 18. Representative fit of Eq. 19 to an NCl(a) deacy curve

From analyses of seven decay curves we obtained a value for the self-annihilation rate constant of $(6\pm1)\times10^{-13}$ cm^3 s^{-1}. We extended this analysis to include data taken under conditions where ClN_3 was not completely dissociated. For this situation we used measurements of the laser power and the published absorption cross section to predict the initial NCl(*a*) concentration. The above calculations suggest that this procedure may overestimate the concentration by about 15%. Analysis of all of the curves that exhibited significant second-order decay components defined a value for k_{17} of $(7\pm2)\times10^{-13}$ cm^3 s^{-1}. The error range given here incorporates the uncertainty in the branching fraction.

Computational models of the NCl(*a*)/I* system are being developed by Tim Madden (AFRL, Kirtland) and Peter Crowel (Logicon RDA, NM). These models have been optimized to reproduce the performance of the azide laser flow facility at Kirtland. Madden has examined the effects of changing the NCl(*a*) self-annihilation rate constant in his CFD model. As expected, attempts to model recent I* gain measurements with a low value for k_9 overestimated the I* density. This problem could be corrected by reducing the branching fraction for the energy transfer step NCl(*a*)+I→NCl(*X*)+I*, which is not a well-defined parameter at present.

6. Quenching of I* by ClN_3 and HN_3.

A previous study[29] of the quenching of I* by ClN_3 provided a rate constant of 2×10^{-11} cm^3 s^{-1}. This value was found to be incompatible with the data obtained by photolyzing $He/ClN_3/I_2$ mixtures, as described above. To further investigate this conflict we measured the quenching rate constant. In these experiments I* was generated in the presence of ClN_3 by photolysis of I_2. A pulsed dye laser operating at 490 nm was used to dissociate I_2 via the *B-X* continuum. Potential complications from secondary photochemical reactions were avoided by using low concentrations of I_2 and I*. The partial pressure of I_2 in the photolysis cell was held at 15 mTorr and the laser intensity (1.3 mJ cm^{-2}) was sufficient to produce an I* density of approximately 2×10^{12} cm^{-3}.

Fluorescence from I* was selected by a 0.25 m monochromator and detected by a cooled Ge device (ADC model 403). This detector was not fast enough to resolve the time dependence of the I* signal. Hence, the time-integrated signal was monitored as a function of added quenching agent. To obtain quantitative data using this technique it is necessary to know the effective I* decay rate (mostly determined by the quenching due to undissociated I_2) or to calibrate the measurement using a species that has a well known quenching rate constant. We used the latter approach with O_2 as the calibration species ($k=2.6\times10^{-11}cm^3$ s^{-1} at 298 K). The ClN_3 quenching rate constant was derived from two series of measurements made with the I_2 pressure and laser power held constant. First the I* intensity was

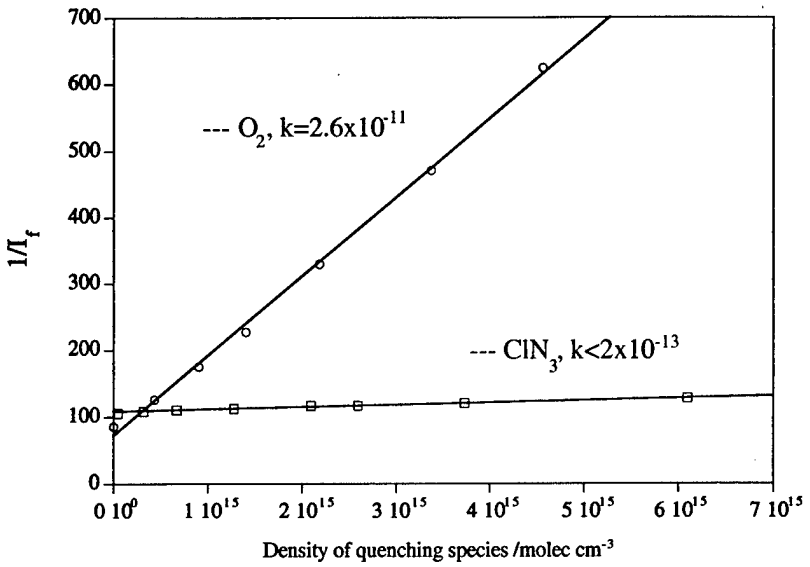

Figure 19. Quenching of $I(^2P_{1/2})$ by ClN_3 and O_2

measured as a function of added ClN_3. The measurements were then repeated with ClN_3 replaced by O_2. Fig. 19 shows typical Stern-Volmer plots (the reciprocal of the fluorescence intensity vs. quenching gas number density) obtained by this procedure. Quenching of I* by ClN_3 was found to be virtually undetectable in these experiments. The slight positive slope of the plot (Fig. 19) is consistent with quenching due to residual Cl_2 from the ClN_3 generator. Comparison with the quenching by O_2 placed an upper limit on the rate constant for quenching by ClN_3 of $k_{16}<2x10^{-13}$. This upper bound is considerably greater than the rate constant used to model the ClN_3/I_2 photolysis experiments. Unfortunately we could not refine this limit, as we were unable to remove all of the residual Cl_2 from the ClN_3 generator or accurately quantify the amount of Cl_2 present. It is evident, however, that our results do not agree with the previous measurement. The origin of this large discrepancy is unclear. Ray and Coombe[29] used 248 nm photolysis of CF_3I to generate I* in the presence of ClN_3. The quenching rate constant was obtained from a plot of the I* decay rate vs. ClN_3 pressure. There is no obvious reason why this approach should yield an erroneous value for the rate constant.

Quenching of I* by HN_3 is of interest as it is thought that residual HN_3 is present in the downstream region of the azide laser flow facility. We used the techniques described above to determine a room temperature rate constant for quenching by HN_3 of $5.8x10^{-13}$ $cm^3\ s^{-1}$.

7. Ab initio calculations for I+NCl energy transfer *(collaboration with Prof. K. Morokuma)*

The energy transfer process NCl(a)+I → NCl(X) + I* is the pump reaction in the NCl(a)/I laser. The I*/I branching ratio and mechanism of transfer are both issues of relevance to azide-driven laser systems. Following our recent theoretical study of the related process[3], I+O_2(a) → I* + O_2(X), we have calculated potential energy surfaces for the ground and low-lying excited states of I-NCl. High-level methods were used; CASSCF and CASPT2, with triple-zeta polarized basis sets. The basis included diffuse orbitals and a relativistic effective core potential for iodine. Calculations that included spin-orbit coupling were carried out with the NCl bond distance fixed at the NCl(a) equilibrium separation (3.0 bohr). The results were very much like those obtained for I+O_2. With the NCl bond frozen, there are no deeply bound states that correlate with NCl(a)+I($^2P_{3/2}$) or NCl(X)+I($^2P_{1/2}$). Figure 20 shows one-dimensional cuts through the surfaces that correlate with these limits. The angle chosen for these cuts (130°) gives the deepest minima and lowest energy curve crossings. As in the case of I+O_2, we found curve crossings below the dissociation asymptote for NCl(a)+I($^2P_{3/2}$). Other curve crossings were evident at higher energies. Recent measurements of the temperature dependence of the NCl(a)+I transfer rate constant[30] yielded an effective activation energy of about 750 cm^{-1}. This suggests that the higher energy surface crossings are important energy transfer channels.

The energy defect for NCl(a) + I transfer is relatively large (1677 cm^{-1}), and near-resonant transfer would be expected to produce vibrationally excited NCl(X, v=2). If the interaction between NCl and I is primarily physical (i.e., processes occurring on potential energy surfaces that are not significantly bound, as suggested by Figure 20), it is unlikely that transfer will occur with simultaneous vibrational excitation of NCl(X). For this situation the excess energy would be released to translational recoil, which is a dynamically unfavorable process. Conversely, if transfer involves the transient formation of a bound INCl complex, the excess energy may be imparted to NCl(X) vibration and/or rotation.

Using spin-free methods we have searched for bound states that correlate with NCl(a) + I by varying all three internal coordinates. Van der Waals minima were located, but none of the potential surfaces supported chemically bound states. This indicates that transfer is mediated by physical interactions. However, to be certain of this result, the calculations need to be extended to include spin-orbit coupling. The ground state surface (correlating with NCl(X)+I) does exhibit a deep minimum when the NCl bond is allowed to extend. If spin-orbit coupling is strong enough, some of this bonding character could be mixed in to the excited states. Calculations where all three coordinates are varied, with inclusion of spin-orbit coupling, will be carried out in the near future.

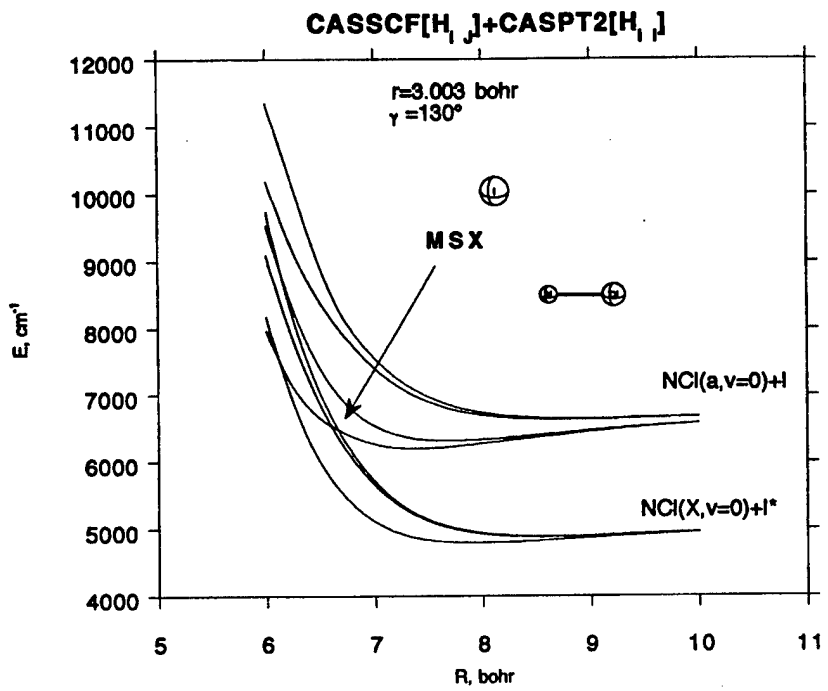

Figure 20. Potential energy curves for INCl

8. Ab initio calculations for Cl + N_3 → NCl + N_2 *(collaboration with Prof. K. Morokuma)*

The reaction Cl + N_3 → NCl + N_2 is known to give substantial yields of NCl(*a*). The potential use of this reaction in a chemically driven iodine laser system is currently being evaluated. The branching ratio for Cl + N_3 → N_2 + NCl(*a, b*) (singlet product) vs. Cl + N_3 → N_2 + NCl(*X*) (triplet product) is a critical issue for laser pumping applications. In recent kinetic studies it has been determined that NCl(*a*) is formed with a yield in excess of 60%[31]. However, it is a difficult matter to make a direct experimental determination of the branching ratio. To address this issue we are performing *ab initio* calculations to examine the singlet/triplet branching ratio from a theoretical perspective. Qualitative features of the potential energy surfaces have been investigated using the B3LYP/6-31+G(d) level of theory. Improved energies for the stationary points were then computed using CASSCF (12 electrons, 10 orbitals) followed by CASPT2 (8 electrons, 6 orbitals). The basis set used was of valence triple zeta quality (*spdf, sp+*). Figure 21 shows a summary of the results (with the singlet and triplet states denoted by S_0 and T_1). The left and right hand sides of this figure correspond to reactants and products, respectively. The minimum energy structure for N_3Cl was found about ~40 kcal/mol below the entrance channel. There is no barrier between this minimum and the Cl + N_3 reactants side, but a barrier exists between N_3Cl and the products NCl(*a*)+N_2 on the siglet surface. As can be seen in Figure 21,

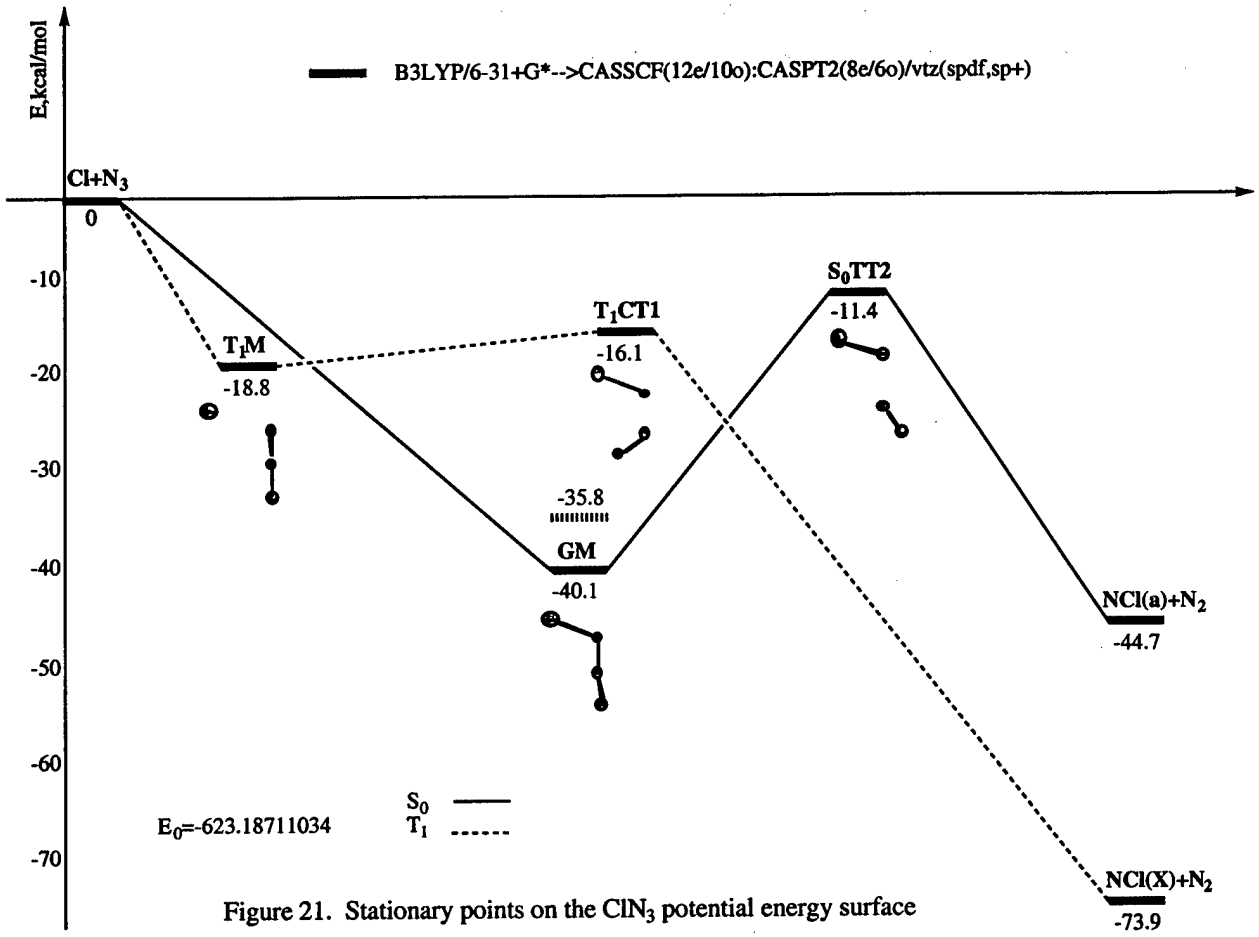

Figure 21. Stationary points on the ClN_3 potential energy surface

this barrier, which corresponds to a *trans* structure, lies 11 kcal/mol below the $Cl+N_3$ entrance channel, but 33 kcal/mol above the singlet products. The triplet surface has a shallower minimum than S_0, lying about ~19 kcal/mol below $Cl + N_3$. There is no barrier on the triplet surface between $Cl+N_3$ and the minimum energy structure for triplet N_3Cl, but a small barrier (2 kcal/mol) exists between $N_3Cl(T_1)$ and the products $NCl(X^3\Sigma^-) + N_2$, The minimum point on the S_0/T_1 surface of crossing (MSX) occurs before the S_0 exit barrier but just after the T_1 exit barrier, and is located ~1 kcal/mol below the singlet barrier. As the barriers on both the singlet and triplet surfaces lie below the $Cl+N_3$ entrance channel, the reason for the preference for singlet products is not obvious. Preliminary 4-dimensional scans of the surfaces were performed at a lower level of theory (CASSCF/cc-vtz) in order to investigate their topological features. Inspection of these surfaces suggests that the entrance channel for reaction on the singlet surface includes a greater range of phase space

than the entrance for the triplet channel. This difference could account for the observed branching ratios, but dynamical calculations are needed to test this notion.

9. References

1 T. Van Marter and M. C. Heaven, *J. Chem. Phys.* **109,** 9266-9271 (1998).

2 T. A. Van Marter and M. C. Heaven, *Proc. SPIE-Int. Soc. Opt. Eng.* **3612,** 125-134 (1999).

3 A. L. Kaledin, M. C. Heaven, and K. Morokuma, *J. Chem. Phys.* **114,** 215-224 (2001).

4 A. L. Kaledin, M. C. Heaven, and K. Morokuma, *Chem. Phys. Lett.* **289,** 110-117 (1998).

5 P. B. Keating, C. A. Helms, B. T. Anderson, T. L. Rittenhouse, K. A. Truesdell, and G. D. Hager, *Proc. Int. Conf. Lasers* **19th,** 194-201 (1997).

6 M. C. Heaven, *Chemical dynamics in chemical laser media* (World Scientific, 2001).

7 J. S. Paschkewitz and M. C. Heaven, *Proc. SPIE-Int. Soc. Opt. Eng.* **3931,** 169-178 (2000).

8 A. J. Bouvier, R. Bacis, A. Bouvier, D. Cerny, S. Churassy, P. Crozet, and M. Nota, *Proc. SPIE-Int. Soc. Opt. Eng.* **1810,** 493-6 (1993).

9 T. L. Henshaw, G. C. Manke, II, T. J. Madden, M. R. Berman, and G. D. Hager, *Chem. Phys. Lett.* **325,** 537-544 (2000).

10 J. M. Herbelin, T. L. Henshaw, B. D. Rafferty, B. T. Anderson, R. F. Tate, T. J. Madden, G. C. Manke, II, and G. D. Hager, *Proc. Int. Conf. Lasers* **21st,** 252-256 (1999).

11 A. J. Ray and R. D. Coombe, *J. Phys. Chem.* **99,** 7849-52 (1995).

12 A. J. Ray and R. D. Coombe, *J. Phys. Chem.* **98,** 8940-5 (1994).

13 T. L. Henshaw, S. D. Herrera, G. W. Haggquist, and V. A. Schlie, *J. Phys. Chem. A* **101,** 4048-56 (1997).

14 K. B. Hewett, G. C. Manke, II, D. W. Setser, and G. Brewood, *J. Phys. Chem. A* **104,** 539-551 (2000).

15 A. V. Komissarov, G. C. Manke, II, S. J. Davis, and M. C. Heaven, *Proc. SPIE-Int. Soc. Opt. Eng.* **3931,** 138-148 (2000).

16 T. Van Marter, M. C. Heaven, and D. Plummer, *Chem. Phys. Lett.* **260,** 201-207 (1996).

17 J. P. Pique, F. Hartmann, R. Bacis, S. Churassy, and J. B. Koffend, *Phys. Rev. Lett.* **52,** 267-70 (1984).

18 J. C. Tully, *J. Chem. Phys.* **93,** 1061 (1990)

19 G. P. Perram and G. D. Hager, (Air Force Weapons Lab.,Kirtland AFB, NM,USA., (1988), 33 pp.

20 G. P. Perram, *Int. J. Chem. Kinet.* **27,** 817-28 (1995).

21 R. F. Heidner, III, C. E. Gardner, G. I. Segal, and T. M. El-Sayed, J. Phys. Chem. **87**, 2348 (1983)

22 W. G. Lawrence, T. A. Van Marter, M. L. Nowlin, and M. C. Heaven, *J. Chem. Phys.* **106,** 127-141 (1997).

23 J. Tellinghuisen and L. F. Phillips, *J. Phys. Chem.* **90,** 5108 (1986).

24 A. V. Kommisarov, V. Goncharov, and M. C. Heaven, in XIII International Symposium on Gas Flow and Cheical Lasers (SPIE, Florence, Italy, 2000).

25 M. Macler, J. P. Nicolai, and M. C. Heaven, *J. Chem. Phys.* **91,** 674-82 (1989).

26 R. Colin and W. E. Jones, *Can. J. Phys.* **45,** 301 (1967).

27 M. A. A. Clyne, A. J. MacRobert, J. Brunning, and C. T. Cheah, *J. Chem. Soc., Faraday Trans. 2* **79,** 1515-24 (1983).

28 M. A. A. Clyne and A. J. MacRobert, *J. Chem. Soc., Faraday Trans. 2* **79,** 283-93 (1983).

29 A. J. Ray and R. D. Coombe, *J. Phys. Chem.* **97,** 3475-9 (1993).

30 T. L. Henshaw, S. D. Herrera, and L. A. Schlie, *J. Phys. Chem. A* **102,** 6239-46 (1998).

31 G. C. Manke, II and D. W. Setser, *J. Phys. Chem. A* **102,** 7257-7266 (1998).

10. Publications Resulting from AFOSR support

1. A. L. Kaledin, M. C. Heaven, and K. Morokuma, Chem. Phys. Lett. **289**, 110 (1998)
   "Ab initio Potential Energy Surfaces for the $I(^2P_{3/2})+O_2(a^1\Delta_g) \leftrightarrow I(^2P_{1/2})+O_2(X^3\Sigma_g^-)$ Energy Transfer Process"

2. T. A. Van Marter and M. C. Heaven, *J. Chem. Phys.* **109**, 9266 (1998).
   "$I(^2P_{1/2})+O_2$: Studies of low temperature electronic energy transfer and nuclear spin state changing collisions"

3. T. A. Van Marter and M. C. Heaven, *Proc. SPIE-Int. Soc. Opt. Eng.* **3612**, 125 (1999)
   "$I(^2P_{1/2})+O_2$: Studies of low temperature electronic energy transfer and nuclear spin state changing collisions"

4. A. L. Kaledin, M. C. Heaven, K. Morokuma, and D. M. Neumark, *Chem. Phys. Lett.* **306**, 48 (1999).
   "Cl_3^- electron photodetachment spectrum: measurement and assignment"

5. M. C. Heaven in "Chemical Dynamics in Extreme Environments", Edited by R. A. Dressler, Advanced Series in Physical Chemistry, World Scientific. In Press.
   "Chemical dynamics in chemical laser media"

5. J.S. Paschkewitz and M. C. Heaven, Gas and Chemical Lasers and Intense Beam Applications: SPIE Proceedings vol. **3931A**, 169 (2000)
   "The COIL chemical kinetics package revisited: a computational investigation of the role of electronically excited states of molecular iodine"

7. A. V. Komissarov, G. C. Manke, S. J. Davis and M. C. Heaven, Gas and Chemical Lasers and Intense Beam Applications: SPIE Proceedings vol. **3931A**, 138 (2000)
   "Kinetic spectroscopy of NCl"

8. A. V. Komissarov, V. Goncharov, and M. C. Heaven, Proceedings of XIII International Symposium on Gas Flow and Chemical Lasers, Florence, Italy, 2000.
   "Chemical Oxygen Iodine Laser Kinetics and Mechanisms"

9. A. L. Kaledin, M. C. Heaven, and K. Morokuma, *J. Chem. Phys.* **114**, 215 (2001)
   "Theoretical Prediction of the Rate Constant for $O_2(a)+I$ Energy Transfer: A Surface-Hopping Trajectory Study"